Chemical Geology 560 (2021) 119981

Contents lists available at ScienceDirect

Chemical Geology

journal homepage: www.elsevier.com/locate/chemgeo

Viscosity of Palmas-type magmas of the Paraná Magmatic Province (Rio Grande do Sul State, Brazil): Implications for high-temperature silicic volcanism

D. Giordano [a,b,c,*], A. Vona [d], D. Gonzalez-Garcia [a], A. Allabar [e], S. Kolzenburg [f,g,h], L.A. Polo [c], V. de Assis Janasi [c], H. Behrens [i], C.P. De Campos [c,h], S. De Cristofaro [a], L. Freitas Guimarães [c], M. Nowak [e], D. Müller [h], A. Günther [h], M. Masotta [j], M. Roverato [k], C. Romano [d], D.B. Dingwell [h]

[a] Dipartimento di Scienze della Terra, Università degli Studi di Torino, Via Valperga Caluso 35, 10125, Turin, Italy
[b] Instituto di Geoscienze e Georisorse, (IGG), Centro Nazionale delle Ricerche (CNR), Pisa, Italy
[c] Instituto de Geociências, Universidade de São Paulo, Rua do Lago, 562 – Cidade Universitária, São Paulo, SP, CEP: 05508-080, Brazil
[d] Dipartimento di Scienze, Università degli Studi Roma Tre, L. go San Leonardo Murialdo 1, 00146, Rome, Italy
[e] Department of Geosciences, Eberhard Karls University Tübingen, Wilhelmstraße 56, 72074 Tübingen, Germany
[f] Department of Geology, 126 Cooke Hall, University at Buffalo, North Campus, Buffalo, NY, 14260–4130, United States
[g] Department of Earth and Planetary Sciences, McGill University, 3450 University Street, H3A 0E8 Montreal, Quebec, Canada
[h] Department for Earth and Environmental Sciences, Ludwig-Maximilians-Universität München, Theresienstr. 41/III, 80333, Munich, Germany
[i] Institute für Mineralogie, Leibniz Universität Hannover, Callinstr. 3, D-30167 Hannover, Germany
[j] Dipartimento di Scienze della Terra, Università degli Studi di Pisa, Via S. Maria, 53, 56,126, Pisa, Italy
[k] Department of Earth Sciences, University of Geneva, Switzerland

ARTICLE INFO

Keywords:
Viscosity measurements
VFT modelling
Paranà Volcanic Products
Brazil

ABSTRACT

This paper provides a new parameterization of the temperature and H_2O content dependence of the pure liquid viscosities of rhyolitic and dacitic magmas associated with representative volcanic products of the Caxias do Sul and Santa Maria eruptive sequences. The viscosities of silicic volcanic products from the Santa Maria rhyolite (SMr), Caxias do Sul (CSd) and Barros Cassal (BCd) eruptive sequences (Lower Cretaceous volcanism of Parana-Etendeka Large Igneous Province) were measured in the temperature range from ca. 1600 °C to the glass transition (T_g). Anhydrous melt viscosities of representative samples from the main eruptive sequences were determined via concentric cylinder viscometry in the superliquidus regime. The quench products of SMr and CSd were then hydrated using an Internally Heated Pressure Vessel to generate two suites of samples with variable water content of up to 4.41 (CSd) and 5.27 (SMr) wt% as determined by Karl Fischer Titration (KFT). Finally, both anhydrous and hydrous samples were used for micropenetration viscosity measurements near T_g. Both types of samples show a minor amount of Fe-Ti-oxide nanolites identified via Raman spectroscopy, which presence did not substantially interfere with viscosity determinations. Based on the results of the viscosity measurements we parameterized the viscosity dependence as a function of water content using the following Vogel Fulcher Tammann (VFT) expressions accounting for the water and temperature dependence of the viscosity:

$\log\eta = -4.55 + (10065–176*H_2O)/[T-(34.6 + 375.3/(1 + H_2O))]$ for SMr.

and

$\log\eta = -4.55 + (9213–338.1*H_2O)/[T-(148.5 + 301.3/(1 + H_2O))]$ for CSd.

where η is the viscosity in Pa s, T the absolute temperature and H_2O the dissolved water content in wt%. This novel parameterization appears to solve a few inconsistencies associated with the variation of the main descriptive parameters of the effect of H_2O, improving the performance of some previous parameterizations. These results are useful for scaling to the conditions extant during ascent and eruption and during flow, emplacement and welding, at temperatures above T_g, for the dacitic and rhyolitic products investigated here.

* Corresponding author.
E-mail address: daniele.giordano@unito.it (D. Giordano).

https://doi.org/10.1016/j.chemgeo.2020.119981
Received 2 April 2020; Received in revised form 26 October 2020; Accepted 5 November 2020
Available online 11 November 2020

1. Introduction

Magma viscosity exerts a fundamental control on most magmatic and volcanic processes, including melt segregation and transport from their source regions, injection and mixing, eruptive style and emplacement dynamics. The rates of these processes varies as a function of temperature, melt composition, water content, vesicularity and crystallinity, driving stresses and strain localisation (e.g. Papale, 1999; Polacci et al., 2004; Cassidy et al., 2018). Generally, low viscosity magmas tend to develop effusive volcanism, while high viscosity magmas ($> 10^6$ Pa s) commonly erupt explosively (Gonnermann and Manga, 2007). Knowledge of the viscosity of eruptive products as a function of temperature and volatile content may help to characterize the eruption dynamics and inform numerical simulations. However, several are the parameters governing the evolution of eruptive events. In fact, volcanic systems are dynamic and controlled by several interrelated processes (e.g. diffusion, crystallization, degassing, permeability development, decompression, cooling) that can indirectly influence the rheological characteristics of magma, resulting in non-linear behaviour during eruption.

The Lower Cretaceous Paraná Etendeka Magmatic Province (PEMP) (131–134 Ma; Ernesto et al., 1999; Thiede and Vasconcelos, 2010; Janasi et al., 2011; Florisbal et al., 2014) (Fig. 1) has one of the greatest preserved volumes (~1Mkm^3) and areal extents (~1.7 Mkm^2) of dominantly basaltic composition of all Large Igneous Provinces (LIPs) on Earth. The South American part of the province, hereafter referred to as PMP (Paraná Magmatic Province), covers an area of at least ca. 917,000 km^2 of the continent with preserved volumes of 450,000 km^3 of extrusive rocks and 112,000 km^3 of intrusive rocks (Frank et al., 2009).

Tholeiitic sequences of basaltic to andesitic lavas, dykes and sills, comprise ~97% of the magmatic volume while only ~3 vol% are silicic volcanic rocks. Amongst the latter, the low-Ti Palmas-type dacites and rhyolites comprise 80% of the total volume of silicic rocks and are associated with the upper sequences of low-Ti basalts at the southern portion of the province (Nardy et al., 2008) with a preserved area of ~63,000 km^2 and thicknesses up to 400 m (Bellieni et al., 1986). Silicic products of Palmas-type are reported to occur as extensive tabular bodies and are subdivided into the lower dacites (Caxias do Sul, Anita Garibaldi, Jacuí, Barros Cassal) and the upper rhyolites (Santa Maria and Clevelândia) (Peate et al., 1992; Peate, 1997; Garland et al., 1995; Nardy et al., 2008; Polo and Janasi, 2014).

Although these silicic products are well characterized geochemically, their eruptive style is still a matter of debate. Determining which deposits are the results of a specific eruption and assessing the associated volume of erupted products is quite complex in LIPs due to exposure problems related to, amongst the others, tectonic activity, erosion and the great extension (10^4 to 10^6 km^2) of frequently thin units. Although unequivocal clastic textures are rare, the huge volumes and the low aspect ratio of part of the volcanic deposits (frequently attributed to fragmental origins and as consequences of explosive activity; e.g. Henry and Wolff, 1992; Branney et al., 2004; Roverato and Giordano, 2016, Roverato et al., 2019), complicate the distinction between volcaniclastic material and banded lava flows and lava-like rheomorphic sequences (Marsh et al., 2001; Bryan et al., 2010; Waichel et al., 2012; Roverato and Giordano, 2016; Roverato et al., 2019; Luchetti et al., 2018a, 2018b; Polo et al., 2018a; Guimarães et al., 2018a, 2018b; Simões et al., 2018b; Andrews et al., 2008; Andrews and Branney, 2005; Andrews et al., 2008). Additional challenges arise from: 1) the lack of pristine textures, 2) strong devitrification of primary volcaniclastic features, 3) hydrothermal alteration; 4) weathering, and 5) the lack of geophysical data in the Brazilian target region.

In the last two decades several authors have reported the occurrence of features typical of an effusive character for the silicic volcanic deposits found in southern Brazil, such as lava fields, lava flows and lava domes (Umann et al., 2001; Lima et al., 2012, 2018; Polo and Janasi, 2014; Rossetti et al., 2017; Guimarães et al., 2018a; Polo et al., 2018b). Silicic feeder dykes, of widths of up to at least 25 m, have also been described recently as associated to effusive activity (e.g. Lima et al., 2012, 2018; De Campos et al., 2016; Guimarães et al., 2015, Guimarães et al., 2018a; Guimarães et al., 2019; Cañón-Tapia and Raposo, 2018).

Textural evidence for extensive pristine pyroclastic products is blurred, mostly by the superposition of different processes. However, early and recent works on these deposits (e.g. Bellieni et al., 1986; Whittingham, 1991; Milner et al., 1992, 1995; Roisenberg and Viero, 2000; Marsh et al., 2001; Bryan et al., 2010; Guimarães et al., 2018b;

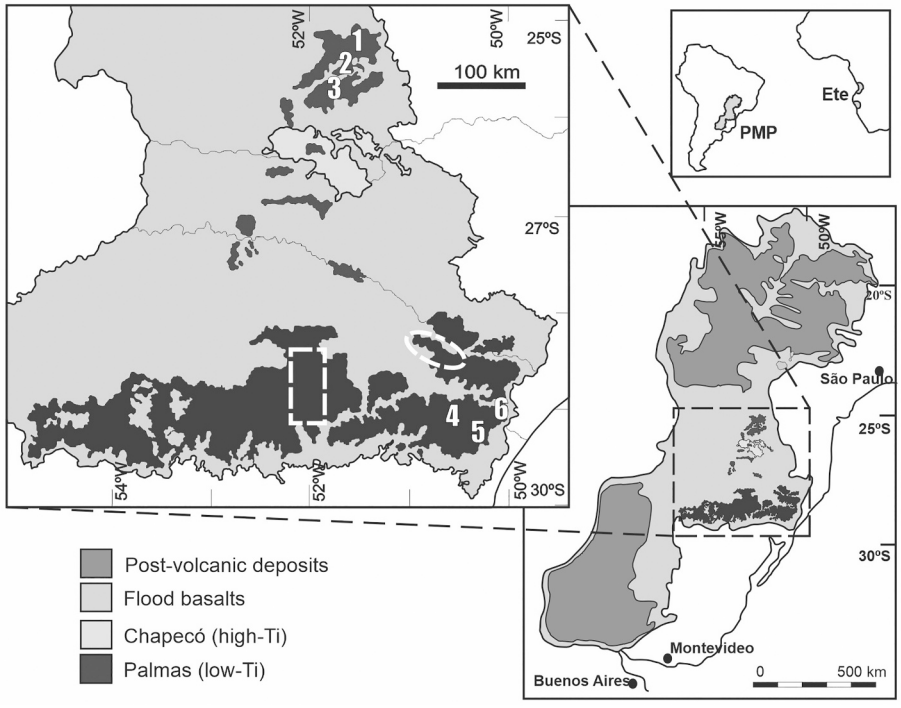

Fig. 1. Summary of the areas investigated by the most recent works. The dashed rectangle corresponds to the area of Gramado Xavier investigated by Polo et al. (2018a, 2018b) while the dashed ellipse corresponds to the area of Sao Marcos already investigated by Lima et al. (2012, 2018), De Campos et al. (2016), Simões et al. (2015, 2018a, b) and Guimarães et al. (2015, 2018, 2019) amongst others. Numbers (from 1 to 6) correspond instead to the areas investigated by Lucchetti et al. (2018).

Luchetti et al., 2018a, 2018b) has pointed out rheomorphic ignimbrite features, typical of lava-like deposits, interlayered with lava flows and domes similar to those reported for other large silicic provinces, such as the Snake River Plain in the US (e.g. Andrews and Branney, 2005). The recognition of rheomorphic ignimbrites has been based primarily on the field observations of: 1) extensive sheet-like horizons of up to 40 km long continuous layers, both in the western and eastern part of the PEMP deposits, 2) the presence of basal vitrophyres and basal baked breccia layers, 3) deformational features such as sheath folds (Andrews and Branney, 2011); and 4) the presence of strongly rotated strain-markers (e.g. crystals and/or lithic clasts). These are features similar to those described in other lava-like deposits (or rheomorphic ignimbrites), which have been primarily generated from welded deposits of fragmental origin which, on the African counterpart of the province, were interpreted as pyroclastic flows (e.g. Owen-Smith et al., 2017 and references therein).

The present picture suggests however a complex eruptive scenario, most probably with the occurrence of different eruptive styles in the same portions of the PMP (e.g. Polo et al., 2018a, 2018b; Guimarães et al., 2018b, 2019) as observed during recent eruptions of silicic products (e.g. Castro et al., 2013; Tuffen et al., 2013).

The pre- and *syn*-eruptive conditions can be better constrained by establishing the quantitative evolution of the transport properties during magma ascent and the emplacement dynamics of volcanic materials, both through field-campaigns and numerical simulation. In these processes, viscosity is arguably the most important property governing the production of silicic melts, as well as their transport to surface and eruption dynamics (e.g., Papale, 1999; Dingwell, 1996; Sparks and Aspinall, 2004; Giordano et al., 2008).

Regardless of the calculations provided by the existing models, we decided to measure the dry and hydrous Newtonian shear viscosity of a Caxias do Sul dacite (CSd) and a Santa Maria rhyolite (SMr) representing the uppermost stratigraphic units of the volcanic sequence. Anhydrous shear viscosities of a dacitic product (BCd) of the older Barros Cassal (BC) sequence were also measured.

Here, a total of 101 new viscosity measurements are provided and compared with data on rhyolitic and dacitic compositions measured in previous contributions (e.g. Giordano et al., 2009; Ardia et al., 2008; Di Genova et al., 2013). Upon previous determination of field evidences of the geometrical features and distribution of eruptive vents (e.g. Lima et al., 2012, 2018; Guimarães et al., 2018a, 2018b; Simões et al., 2018a, 2018b; Polo et al., 2018b) and knowledge of eruptive temperatures and depth of ascending magmas (e.g. Polo et al., 2018a), these measurements can be used to help test whether either an effusive or an explosive behaviour is expected for the investigated magma types.

2. Sample selection and characterization

The samples used in the present experimental study correspond to three silicic units of Palmas-type sequence and are a rhyolite from the SMr unit (~71 wt% SiO_2), a dacitic vitrophyre from the CSd unit (~69 wt% SiO_2), and a dacitic vitrophyre (RS73a) collected from the Barros Cassal units (64–66 wt% SiO_2) (Fig. 2). The selected samples are compositionally homogeneous and constitute the majority of the products erupted during the above-mentioned Palmas-type volcanism. All samples analyzed here were collected in the area mapped by Polo and Janasi (2014) and Guimarães et al. (2018a) at the southern border of PMP in the Rio Grande do Sul state, Brazil, and are considered the most representative compositions of each unit (Polo et al., 2018a, 2018b).

The CSd samples employed here, referred as GX07 and SM01D, were near the localities of Gramado Xavier and São Marcos, respectively (Polo and Janasi, 2014 and Guimarães et al., 2018b; Fig. 1). GX07 was collected from a lava dome and has a vitrophyric texture with up to 10 vol% of phenocrysts (Fig. 2): plagioclase ($An_{52–67}$), augite, orthopyroxene and Ti-magnetite often forming a glomero-porphyritic texture set in a glassy matrix. The glass matrix shows no evidence of macroscopic alteration (Polo et al., 2018b). SM01D corresponds to the basal glassy layer of the deposits interpreted by Guimarães et al. (2018b) as rheoignimbrites and contains a low microlite content (< 1 vol%; plagioclase, pigeonite and Ti-magnetite). Clusters of euhedral crystals of plagioclase, pyroxene and magnetite occur locally (Fig. 2). The crystal assemblage of CSd samples does not contain quartz or hydrous phases (e.g. amphibole). The samples of the SMr unit, referred to as RS74 and RS74L, were collected from the deposits of banded flows (lava flow with banding and extensive flows of SM) next to the locality of Gramado Xavier (Polo and Janasi, 2014). These samples are characterized by

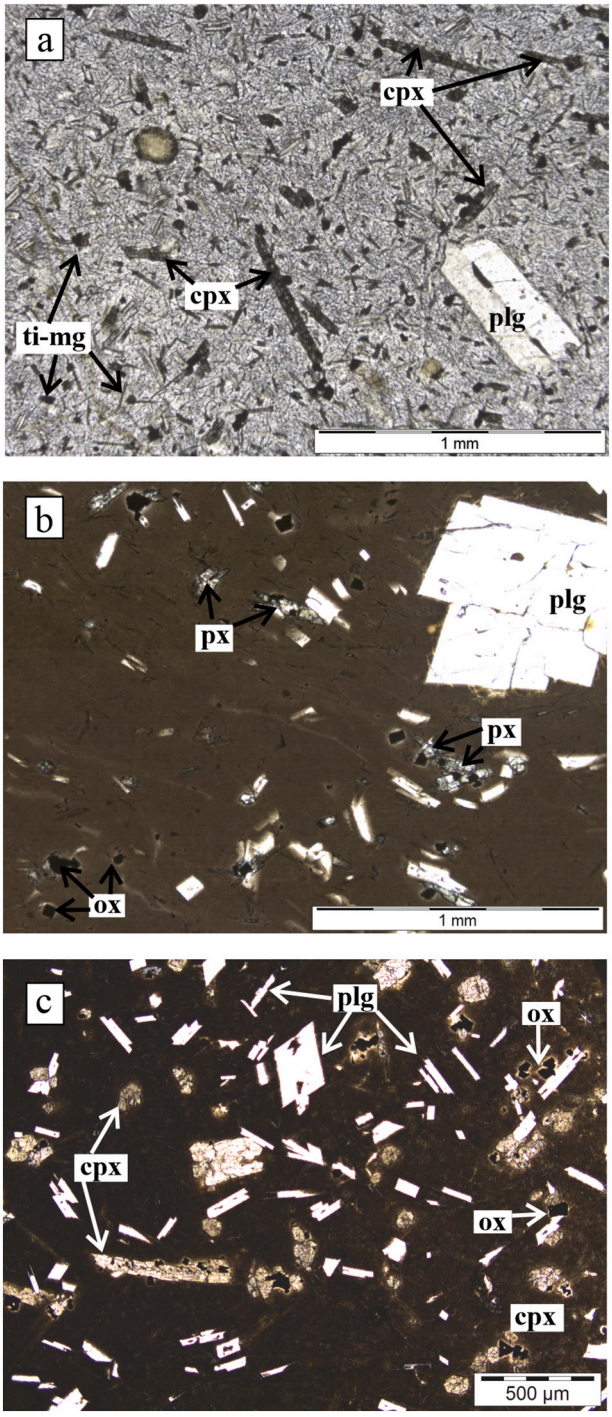

Fig. 2. Transmitted light microphotographs of characteristic samples from SMr (a); CSd (b) and BCd (c). Abbreviations: ox (Fe-Ti-oxides), plg (plagioclase); cpx (clynopryroxene); ox (orthopyroxene).

Table 1
Compositional details of glasses of the investigated natural and remelted volcanic samples.

		SiO_2	TiO_2	Al_2O_3	FeO_{tot}	MnO	MgO	CaO	Na_2O	K_2O	P_2O_5	Cr2O3	Cl	SO2	Location	SiO_2 norm	Alkali norm
Remelted glass compositions																	
Santa Maria	RS74	72.1	0.7	12.8	4.8	0.1	0.6	2.3	3.4	3.8	0.2				Gramado Xavier	71.52	7.10
Santa Maria	RS74L	71.71	0.70	12.61	4.67	0.11	0.65	2.27	3.17	3.70	0.01	0.01	0.01	0.01	Gramado Xavier	72.00	6.90
Caxias do Sul	GX07	67.0	1.0	12.6	5.8	0.1	1.3	3.3	3.3	2.9	0.2				Gramado Xavier	68.65	6.33
Caxias do Sul	SM01D	69.90	0.91	13.19	5.16	0.12	1.23	3.32	3.19	3.10	0.02	0.01	0.01	0.01	Sao Marcos	69.80	6.28
Barros Cassal	RS73a	63.6	1.3	12.8	8.4	0.2	1.7	4.5	3.2	2.5	0.3				Gramado Xavier	64.50	5.78

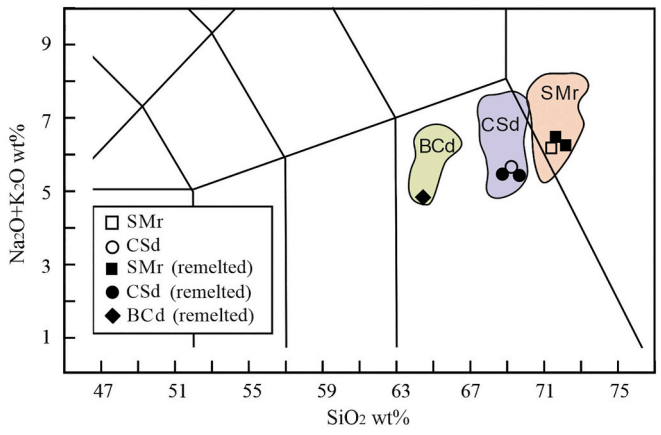

Fig. 3. Total Alkali Silica (TAS) diagram for SMr and CSd samples collected in Gramado Xavier and Sao Marcos (see more details in Polo et al., 2008; Guimarães et al., 2018b) and the Fe-rich Barros Cassal dacite (BCd) (Table 1). Contoured grey areas correspond to the range of variability of compositions associated to the main volcanic sequences (e.g. Polo et al., 2018a).

partially devitrified vitrophyres (e.g. vitrophyric lavas or rheomorphic ignimbrite material with obliterated textures), with phenocrysts (<5%), microphenocrysts (<5%) and microlites (<20%) of plagioclase ($An_{39–57}$), Ti-magnetite and pigeonite (Fig. 2).

The Barros Cassal dacite (RS73a) was collected from a lava flow deposit next to Gramado Xavier (Polo and Janasi, 2014) and is a vitrophyric sample with up to 15 vol% of crystals of andesine-labradorite (An47–53), augite and Ti-magnetite (Fig. 2c). Further compositional and petrographic details of the investigated products can be found in Polo et al. (2018a, 2018b). All selected rocks are representative of typical Palmas-type silicic volcanism in terms of their compositions, frequency, distribution and size of the investigated outcrops and the overall similarity of petrological characteristics (Polo and Janasi, 2014; Polo et al., 2018a, 2018b).

Both the residual glass matrix composition of the SMr and CSd natural samples (RS74L and SM01D) and remelted whole rock compositions of RS74, RS74L, GX07, SM01D and RS73a are reported in Table 1 and Fig. 3. The BCd is more mafic than CSd, with less SiO_2 and alkalis, and higher MgO, CaO and FeO_{tot} content. Details of the measuring conditions are reported in the Appendix (§ A.0).

3. Experimental and analytical rationale

The anhydrous starting materials here investigated experimentally were obtained by direct fusion of total rock (TR) samples for the Caxias do Sul dacite (GX07), Santa Maria rhyolite (RS74), and Barros Cassal dacite (RS73a) eruptive sequences. A concentric cylinder (CC) apparatus (Dingwell et al., 1996) was used for sample homogenization and determination of anhydrous liquid viscosities ($10^{2.1}$–$10^{4.7}$ Pa s, at 1 atm) at *superliquidus* temperature (T = 1148–1591 °C), whereas micropenetration (MP) viscometry was used to measure viscosity in the range between $10^{9.49}$ and $10^{11.25}$ Pa s at temperatures between 419 and 840 °C (§ A.1) in the glass transition interval. Glasses obtained after the concentric cylinder experiments were retrieved by drilling and used for the micropenetration measurements (§ A.2) and for the hydration experiments. Samples of varying water content were synthesized using an internally heated argon pressure vessel (IHPV) at intrinsic oxygen fugacities of ΔlogFMQ between ~ + 2.5–3.5, depending on H_2O content (e.g. Allabar et al., 2020) (details of the methods can be found in the Appendix A.3). The water-bearing glasses were cut into 1–2 mm thick disks, double polished, and stored in a desiccator until further use (e.g. Raman spectroscopy, Karl Fischer Titration, Micropenetration, X- ray diffraction (XRD)).

Water contents of hydrated samples were determined using KFT (Table 2) as reported in Appendix (A4) and homogeneous distribution was confirmed using Raman spectroscopy (Appendix A.5). The doubly polished disks were then used to run micropenetration measurements under Argon atmosphere at 1 atm pressure. Further details of these experimental techniques are summarized in the appendix (A.2.) and follow the approach described in previous studies (e.g., Hess and Dingwell, 1996; Dingwell et al., 1996; Giordano et al., 2004; Giordano et al., 2005).

Finally, we investigated and ruled out the possibility that a certain proportion of nanolites (nano-crystals), present in the hydrated samples, might influence the viscosity determinations in the low temperature interval close to glass transition. The acquisition of this information required the employment of three different techniques: 1) micro-Raman spectroscopy, 2) X-ray diffraction (XRD) and 3) scanning electron microscopy (SEM). A discussion related to the observed physical effects on viscosity measurements due to the crystallization of, at maximum, 1.5

Table 2
Average H_2O content (in wt%) of hydrated samples determined by Karl-Fischer Titration (KFT), based on two measurements for each sample.

Sample Name	Av. values	Av. Uncertainty
	wt%	wt%
RS74–0.5	0.78	0.07
RS74–1	1.21	0.14
RS 74–2	2.12	0.11
Rs-74 - 3	2.98	0.11
RS74–4.5	5.27	0.14
GX-07 - 0.5	0.89	0.10
GX-07 - 1	1.23	0.10
GX-07 - 2	1.95	0.12
GX-07 - 3	3.43	0.12
GX-07 - 4.5	4.41	0.09

wt% of Fe-Ti-oxides is reported in A.6.

Micro-Raman spectroscopy (as reported in Appendix § A.5) was performed on dry and hydrous glasses to check for the presence of nanolites, commonly invisible to other techniques (SEM, XRD), that frequently form in volcanic and synthetic glasses (Di Genova et al., 2017) as a consequence of cooling and alteration. Both anhydrous glasses retrieved after concentric cylinder viscometry, hydration syntheses and micropenetration as well as natural samples (Gonzalez-Garcia et al., 2020 - this issue), show the presence of Raman peaks at around 320 and 670 to 690 cm^{-1} indicative of the presence of Fe—Ti oxide nanolites (Fig. 4). These crystals were only partially resolved by SEM imaging, but remained below detectability of X-ray diffraction analysis (§ A.6) performed at the Department for Earth and Environmental Sciences, LMU Munich. Using the Giordano et al. (2008a) model (hereafter referred to as GRD model), which very well predict the viscosity of measured samples, we also tested the effect on the viscosity of a loss of up to 1.5 wt% of iron (due to formation of nanolites) from the liquid. According to these calculations the low temperature viscosity would increase at maximum up to 0.25 log units at the highest viscosities. This effect was not included in our parameterization.

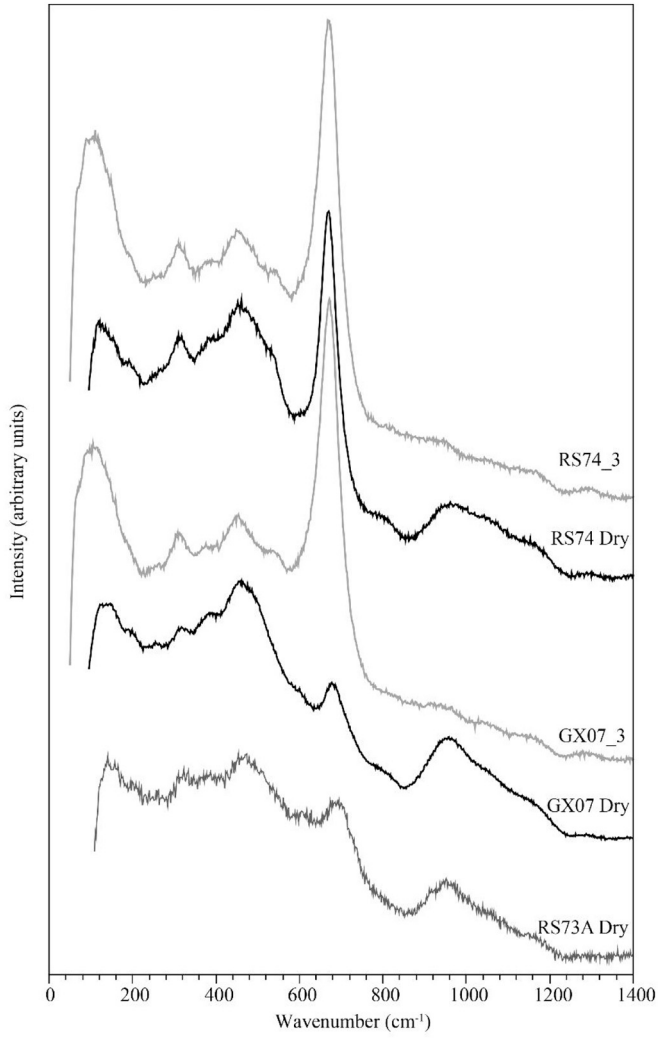

Fig. 4. Examples of Raman spectra of anhydrous GX07_dry, RS74_dry and RS73a_dry samples taken after concentric cylinder viscometry and comparison with hydrous samples GX07_3 and RS74_3 obtained after high-pressure, high temperature synthesis. In addition to the typical broad bands of glasses at 490 cm^{-1} and 960 cm^{-1}, other peaks show up for some of the samples. In particular, the RS74 rhyolite shows well developed peaks at ca. 670 cm^{-1} for both dry and hydrous samples. On the other hand, while the GX07 dry sample has a negligible peak at around 670 cm^{-1}, the GX07–3 has also a well pronounced peak. Finally, the RS73A sample also shows a small peak at ca 690 cm^{-1}. Other minor peaks are observed at ca 310–320 cm^{-1} and 540 cm^{-1}(this latter one only visible in a few samples). Low wavenumber peaks (320 and 540 cm^{-1}) as well as the large peaks at 670–690 cm^{-1} are associated to Fe-Ti-oxides (e.g. De Faria et al., 1997; Di Genova et al., 2017, 2018).

4. Results

4.1. Viscosity results

Viscosity determinations for the dry and hydrous melts are presented in Table 3. The dry viscosity of re-melted bulk rocks of products from the CSd (GX07 and SM01D), SMr (RS74, RS74L) and BCd (RS73a) are presented as a function of reciprocal temperature in Fig. 5. Being the compositions similar, the viscosities of the re-melted samples from the same volcanic sequence (SMr, CSd, BCd) are substantially indistinguishable. Thus, the viscosities from the same stratigraphic unit of the same volcanic sequence are parameterized below.

The SMr sample has a viscosity only slightly higher than the CSd, while CSd has a viscosity about 0.7 log units higher with respect to the BCd sample (Fig. 5). The pattern observed at high temperature is also observed at low temperature approaching the T_g for the SMr and CSd, where no crossovers are observed in the interval of measurement. No low temperature viscosity data were measured for the BCd samples and as a consequence no regression curves are included in the figure for this sample.

The viscosities of dry and hydrous samples from the Caxias do Sul dacite (CSd) and Santa Maria rhyolite (SMr) are shown in Fig. 6 and are reported in Table 3. The viscosity interval experimentally accessible with the micropenetration technique becomes increasingly restricted with increasing water content and decreasing melt polymerisation. This is because above the glass transition interval, the diffusive loss of water from the melt can be significant on the measurement timescale. Note that although viscosity appears to show a nearly Arrhenian behaviour over the restricted range of each individual technique (for each H_2O content), a variable degree of non Arrhenian behaviour (fragility) emerges over the entire temperature range explored. The slope of low – T viscosities appears to slightly decrease with increasing the H_2O content and, as a consequence, fragility decreases (e.g., Giordano et al., 2008; Giordano et al., 2009).

5. Discussion

5.1. Data modelling and comparison with previous models

The viscosity data (Tables 3) were fitted using a Vogel-Fulcher-Tammann (VFT) (Vogel, 1921; Fulcher, 1925; Tammann and Hesse, 1926) expression:

$$log\eta = A_{VFT} + \frac{B_{VFT}}{T(K) - C_{VFT}} \quad (1)$$

where η is viscosity in Pa s, T(K) is the absolute temperature and A_{VFT}, B_{VFT} and C_{VFT} are the pre-exponential factor, the pseudo-activation energy and the VFT temperature, respectively. Fits were performed assuming that A_{VFT} is a constant of −4.55 independent of composition (Russell et al., 2003; Giordano and Russell, 2007; Giordano et al., 2008) and thus, the effect of water is integrated solely into the B_{VFT} and C_{VFT} parameters.

Particular care should be taken when interpreting the fit parameters of the VFT equation. Russell et al. (2002) demonstrated that fitting viscosity–temperature data to non-Arrhenian rheological models can result in strongly correlated or even non-unique, sometimes unphysical, model parameters (A, B, C) of a VFT equation (Eq. (1)). The same authors quantified and discussed the possible sources of error for typical fragile to strong natural silicate melts. This demonstrated that in order to

Table 3
Measured viscosities of the investigated samples at varying temperature and water content.

Sample	SMr					CSd					BCd		
	T(°C)	log [η (Pa s)]	H_2O (wt%)	H_2O (mol%)		T(°C)	log [η (Pa s)]	H_2O (wt%)	H_2O (mol%)		T(°C)	log [η (Pa s)]	H_2O (wt%)
RS74_dry	760.2	11.76	0	0	GX07_dry	800.1	10.32	0	0	RS73a_dry	1483.3	1.94	0
RS74_dry	780.1	10.99	0	0	GX07_dry	840.1	9.54	0	0	RS73a_dry	1459.3	2.045	0
RS74_dry	800.1	10.47	0	0	GX07_dry	740.1	11.77	0	0	RS73a_dry	1435.3	2.16	0
RS74_dry	840.1	9.67	0	0	GX07_dry	760.2	11.36	0	0	RS73a_dry	1411.4	2.28	0
RS74_dry	1296.6	4.04	0	0	GX07_dry	780.1	10.58	0	0	RS73a_dry	1387.4	2.36	0
RS74_dry	1321.1	3.88	0	0	GX07_dry	820.2	9.60	0	0	RS73a_dry	1363.4	2.53	0
RS74_dry	1345.6	3.73	0	0	GX07_dry	1345.6	3.28	0	0	RS73a_dry	1339.4	2.66	0
RS74_dry	1370.1	3.58	0	0	GX07_dry	1370.1	3.14	0	0	RS73a_dry	1315.4	2.79	0
RS74_dry	1370.1	3.58	0	0	GX07_dry	1394.6	3.00	0	0	RS73a_dry	1291.5	2.94	0
RS74_dry	1389.3	3.46	0	0	GX07_dry	1419.2	2.86	0	0	RS73a_dry	1267.5	3.09	0
RS74_dry	1419.2	3.29	0	0	GX07_dry	1443.7	2.73	0	0	RS73a_dry	1243.5	3.24	0
RS74_dry	1443.6	3.16	0	0	GX07_dry	1468.2	2.59	0	0	RS73a_dry	1219.5	3.42	0
RS74_dry	1443.7	3.15	0	0	GX07_dry	1492.7	2.47	0	0	RS73a_dry	1195.5	3.59	0
RS74_dry	1468.2	3.02	0	0	GX07_dry	1492.7	2.47	0	0	RS73a_dry	1171.6	3.78	0
RS74_dry	1492.6	2.90	0	0	GX07_dry	1517.2	2.35	0	0	RS73a_dry	1147.6	3.97	0
RS74_dry	1518.4	2.83	0	0	GX07_dry	1541.7	2.25	0	0				
RS74_dry	1541.7	2.64	0	0	GX07_dry	1541.7	2.24	0	0				
RS74_dry	1541.7	2.64	0	0	GX07_dry	1566.2	2.13	0	0				
RS74_dry	1566.2	2.53	0	0	GX07_dry	1590.7	2.02	0	0				
RS74_dry	1589.6	2.47	0	0	SM01D_dry	1493.00	2.50	0	0				
RS74L_dry	1591.0	2.44	0	0	SM01D_dry	1444.00	2.76	0	0				
RS74L_dry	1542.0	2.67	0	0	SM01D_dry	1395.00	3.03	0	0				
RS74L_dry	1493.0	2.93	0	0	SM01D_dry	1346.00	3.32	0	0				
RS74L_dry	1444.0	3.19	0	0	SM01D_dry	1297.00	3.62	0	0				
RS74L_dry	1395.0	3.48	0	0	SM01D_dry	1248.00	3.94	0	0				
RS74L_dry	1346.0	3.76	0	0	SM01D_dry	1199.00	4.29	0	0				
RS74L_dry	1297.0	4.07	0	0	SM01D_dry	1150.00	4.67	0	0				
RS74L_dry	1248.0	4.41	0	0	GX07_0.5	680.1	9.57	0.89	3.74				
RS74L_dry	1199.0	4.78	0	0	GX07_0.5	660.1	9.87	0.89	3.74				
RS74_0.5	680.1	9.69	0.78	1.78	GX07_0.5	620.1	10.86	0.89	3.74				
RS74_0.5	660.1	10.33	0.78	1.78	GX07_0.5	650.0	10.15	0.89	3.74				
RS74_0.5	620.1	10.89	0.78	1.78	GX07_1.0	620.1	9.66	1.23	4.28				
RS74_1.0	600.1	10.19	1.21	4.22	GX07_1.0	600.1	10.39	1.23	4.28				
RS74_1.0	560.1	11.07	1.21	4.22	GX07_1.0	560.0	11.19	1.23	4.28				
RS74_1.0	620.1	9.73	1.21	4.22	GX07_1.0	590.0	10.49	1.23	4.28				
RS74_2.0	539.9	10.10	2.12	7.23	GX07_2.0	580.1	9.54	1.95	7.24				
RS74_2.0	500.0	11.15	2.12	7.23	GX07_2.0	560.0	10.04	1,95	7.24				
RS74_2.0	560.1	9.52	2.12	7.23	GX07_2.0	520.0	11.08	1.95	7.24				
RS74_3.0	500.0	10.09	2.98	9.96	GX07_3.0	540.1	9.37	3.43	10.91				
RS74_3.0	480.0	10.66	2.98	9.96	GX07_3.0	500.0	10.18	3.43	10.91				
RS74_3.0	520.0	9.62	2.98	9.96	GX07_3.0	480.0	10.86	3.43	10.91				
RS74_4.5	460.0	9.86	5.27	16.69	GX07_4.5	460.0	9.86	4.41	14.61				
RS74_4.5	439.9	10.37	5.27	16.69	GX07_4.5	440	10.04	4.41	14.61				
RS74_4.5	419.9	10.70	5.27	16.69									

have well constrained parameters the data collected preferably over the widest possible range of viscosity through the employment of more than one measure technique (e.g. micropenetration, concentric cylinder, centrifuge falling sphere; Ardia et al., 2008, amongst others) should be combined together. Particular care should also be taken when working with "strong" liquids (having a near Arrhenian rheological behaviour, e.g. Angell, 1985), as the range of the numerically accessible values for parameters A, B and C for these liquids is demonstrated to be 5–10 times greater than the range of values estimated for fragile melts (having a strongly non-Arrhenian rheological behaviour, e.g. Angell, 1985). The smaller or larger uncertainty on fitting parameters will also derive from the small compositional variation (the H_2O content being the most effective one) on the measured values (Table 2). So the uncertainty on the adjustable parameters is the results of the uncertainty propagation of the different analytical methods. In addition, best fit parameters should also have physically meaningful values (e.g. B and C cannot be negative as they are correlated to activation energies and absolute temperatures, respectively). Finally, the validity of the calibrated equation must be verified case by case, in order to prevent unphysical results as, for example, a viscosity increase with addition of water or with temperature increase (Russell et al., 2002). Extrapolation of data outside the experimental range should be avoided.

Problems can arise when employing equations which appeared adequate in previous studies (Giordano et al., 2009; Di Genova et al.,

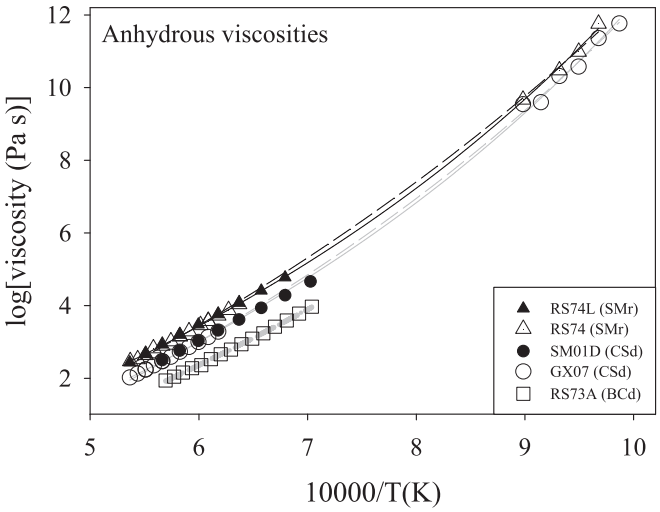

Fig. 5. High and low T viscosity as obtained by using concentric cylinder and micropenetration techniques. The viscosities of dry GX07 and SM01D and RS74 and RS74L were measured for both the SMr (RS74, RS74L) and CSd (GX07, SM01D) samples by independent measurements. The data overlap perfectly in the figures and for that reason they were fitted together to get general trends. Curves in the figures are VFT fits. Fitting parameters are reported in Table 4.

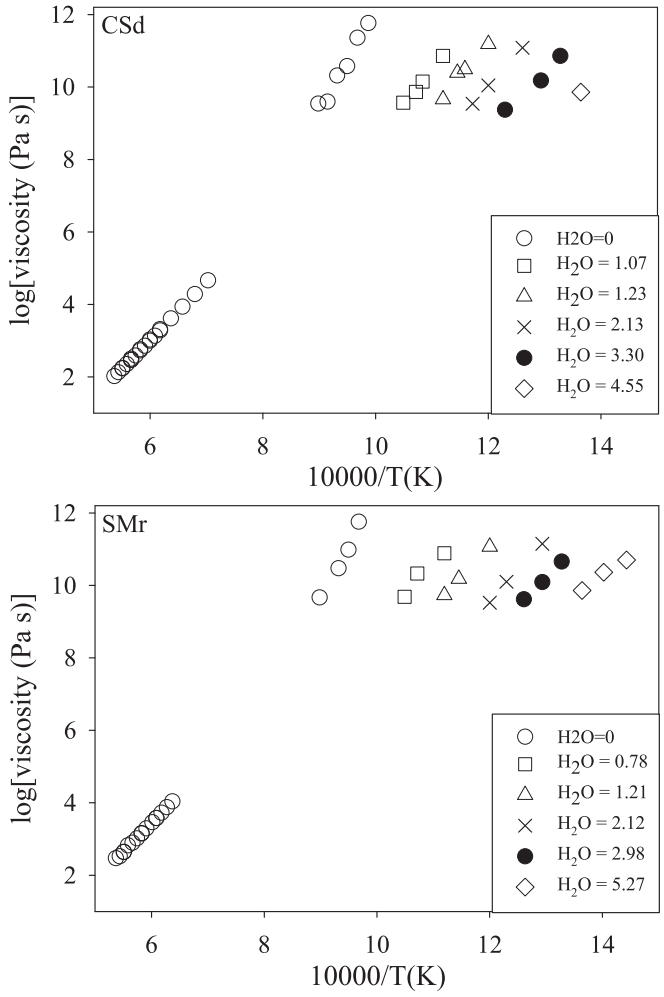

Fig. 6. The high and low temperature viscosity data as a function of H_2O content and the inverse of temperature T(K) are shown in panel a) for the CSd and in panel b) for the SMr. Numbers in the legends indicate the dissolved H_2O content in wt%.

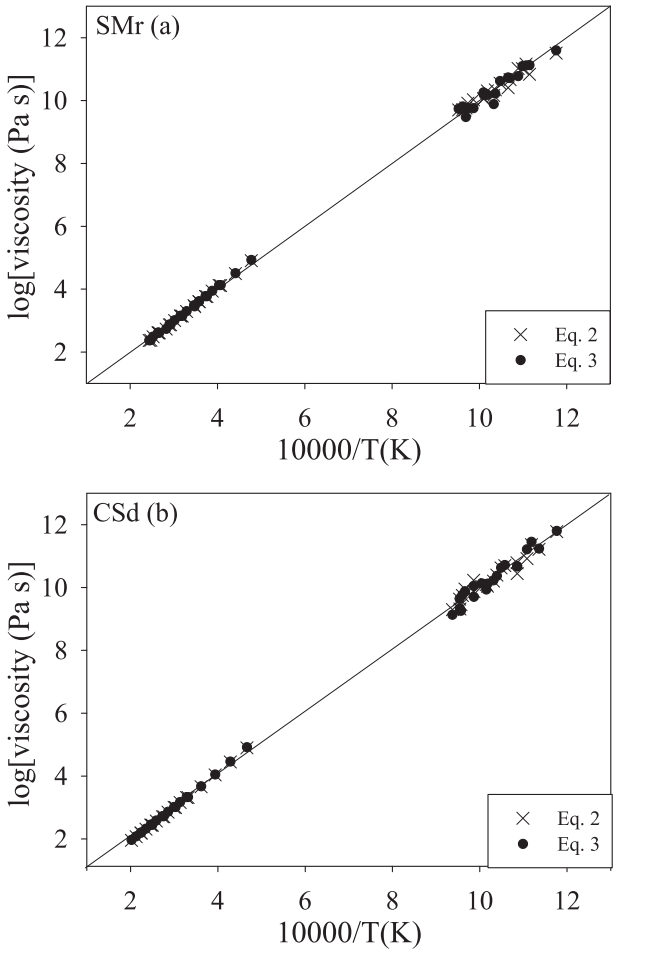

Fig. 7. Calculated viscosity obtained by fitting the VFT expressions of Eqs. 2 and 3 to measured data for the Santa Maria (SMr, panel a) and the Caxias do Sul (CSd, panel b) samples. Fitting parameters are reported in Table 5.

2013). To demonstrate this, we have tested two equation forms expressing the H_2O dependence of the B_{VFT} and C_{VFT} parameters. The first expression (Eq. 2) has the form of that previously employed by Giordano et al. (2009) and Di Genova et al. (2013):

$$\begin{aligned} \mathrm{B_{VFT}} &= B'_{VFT} + B''_{VFT}{*}\mathrm{H_2O} \\ \mathrm{C_{VFT}} &= C''_{VFT} + C''_{VFT} log(1+\mathrm{H_2O}) \end{aligned} \quad (2)$$

while the second expression (Eq. 3), proposed here as an alternative, is such that:

$$\begin{aligned} \mathrm{B_{VFT}} &= B'''_{VFT} + B'^{v}_{VFT}{*}\mathrm{H_2O}. \\ \mathrm{C_{VFT}} &= C'''_{VFT} + C'^{v}_{VFT}/(1+\mathrm{H_2O}) \end{aligned} \quad (3)$$

for both equations, B'^{-IV}_{VFT}, C'^{-IV}_{VFT}, are fit parameters. H_2O of Eq. 2 is the water content in moles % (Giordano et al., 2009), while, for Eq. 3, H_2O is the water concentration in weight percent (wt%).

Fitting of dry and hydrous viscosity data as measured at both high and low T is used to retrieve values of the B_{VFT} *and* C_{VFT} parameters for Eqs. 1 and 2 and Eqs. 1 and 3. Anhydrous samples were all assumed to contain 200 ppm dissolved H_2O (e.g. Hess and Dingwell, 1996). B_{VFT} *and* C_{VFT} parameter values are provided in Table 4 together with their associated uncertainties and RMSE (Root Mean Square Error) values.

Table 4
VFT parameters (A_{VFT}, B'_{VFT}, C'_{VFT}) values.

		A_{VFT}	B'_{VFT}	B''_{VFT}	C'_{VFT}	C''_{VFT}	RMSE	Methods	Model Eq.
HYDROUS	SMr	−4.55	10,098.98	717.96	404.52	−782.41	0.11	HT + LT	Eq. 2
			68.99	40.98	6.04	16.79			
	CSd	−4.55	9195.84	522.68	450.14	−675.16	0.14	HT + LT	Eq. 2
			82.49	63.27	6.72	22.03			
	SMr	−4.55	10,064.92	−175.99	34.60	375.28	0.12	HT + LT	Eq. 3
			74.01	18.89	6.95	7.44			
	CSd	−4.55	9213.04	−338.14	148.49	301.27	0.14	HT + LT	Eq. 3
			81.31	28.64	8.33	8.50			

HT refer to high temperature; LT refer to low temperature.

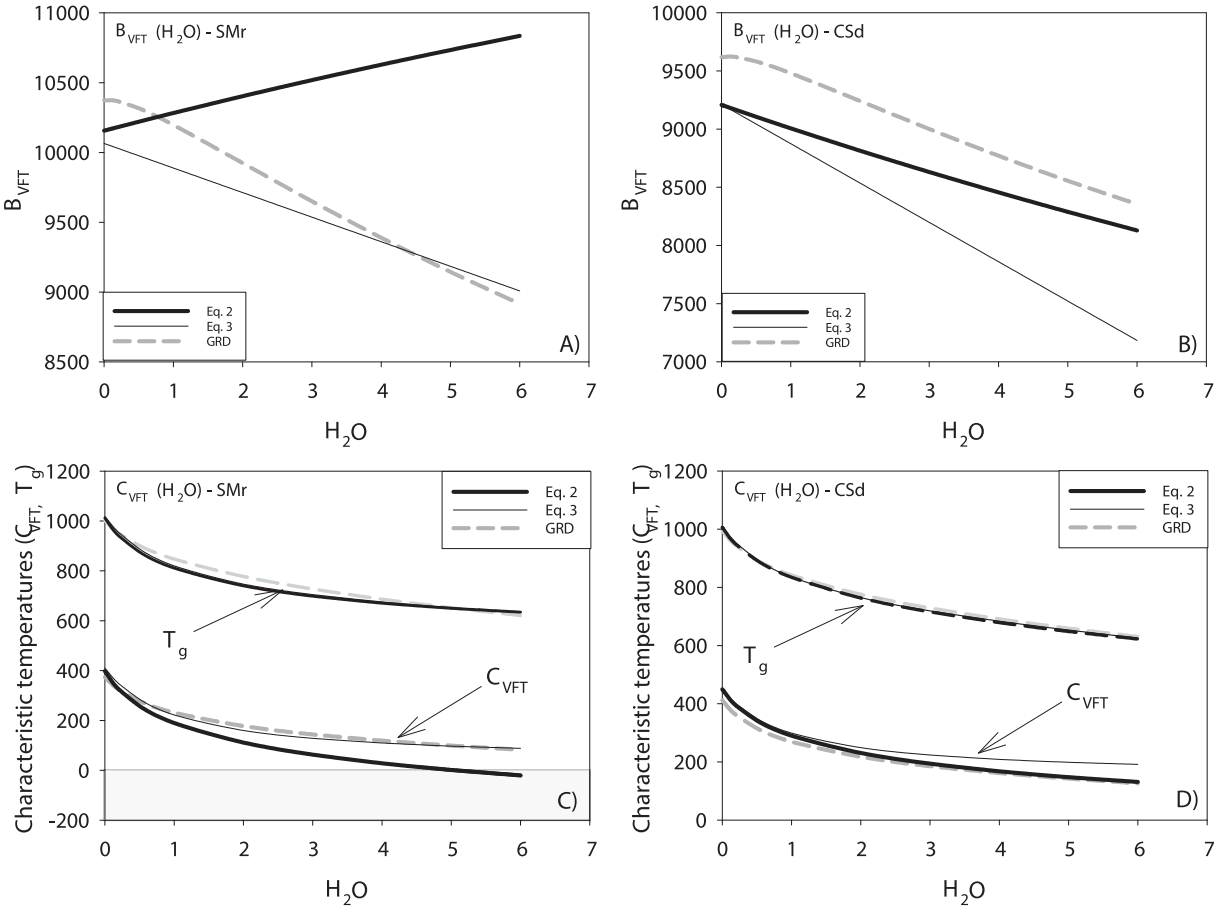

Fig. 8. *B_{VFT} and C_{VFT} parameters and calculated T_g variation as a function of H_2O content (wt%) obtained by using Eq. 2 and Eq. 3 and the GRD model proposed by Giordano et al. (2008). Panels A) and B) show the B_{VFT} – H_2O paths, whereas panels C) and D) show, as a function of the H_2O (wt%), the variation of characteristic temperatures: C_{VFT} (lower curves, as indicated by the arrow) and T_g (upper curves) as calculated for logη = 12. Thick and thin blqack lines are those, respectively associated to Eq. 2 and Eq. 3 models. Thick grey long-dashed curves are those obtained by the employment of the GRD mode. The B_{VFT} and C_{VFT} curve variation as a function of H_2O for the SMr samples are reported in panels A) and C), while panels B) and D) represent the B_{VFT} and C_{VFT} curve variation as a function of H_2O for the CSd samples.*

Table 4 and Fig. 7 indicate that both Eq. 2 and Eq. 3 predict the measured viscosities of both SMr and CSd well. Nonetheless, it is worth noting that, although the viscosity of the investigated melts is numerically well predicted and the calculated glass transition temperatures (T_g) (taken as the temperature at which log η = 12) (Fig. 8 C, D) appear similar when employing Eq. 2 or Eq. 3, an anomalous behaviour of the B_{VFT} and C_{VFT} as a function of water content is observed in the panels of Fig. 8A, B for the SMr sample. In fact, Fig. 8A shows that B_{VFT} may increase with increasing H_2O content if Eq. 2 is used, while it decreases consistently when using Eq. 3.

On the other hand, the variation of C_{VFT} as a function of H_2O content (panels C and D in Fig. 8) shows a smoother trend, levelling off to a constant value if Eqs. 2 and 3 are used, where slightly negative, hence unphysical, absolute temperature values (up to ~ −60 K) is obtained by Eq. 2 (grey shaded area) for the SMr sample.

The pseudo activation energy B_{VFT} trend and the strongly negative C_{VFT} values derived from Eq. 2 do not seem to agree neither with the measured data plotted in Fig. 6 (no significant slope increase is visible) nor with the expected trends described in literature of the composition dependence of viscosity available to date (Giordano et al., 2008a).

Although models for specific compositional suites exist (e.g. Ardia et al., 2008; Romine and Whittington, 2015 (and corrigendum, 2016); Li et al., 2020) the advantage of using a generalized compositional model stems from the fact that the compositional model is based on a single form of equation, thus reducing the uncertainty associated to the employment of different functional forms for each considered compositions. Such a reasoning, with the due differences, is also at the basis of the work published in Giordano et al. (2009), which compared results based on a unique VFT expression.

The comparison between the trends described above and those obtained by employing the GRD model has been investigated here in order to provide the decisive tool to establish which equation to employ to constrain the transport properties of the samples investigated here (N.B.: GRD model predicts the measured viscosity for the CSd and SMr with RMSE of 0.28 and 0.41, respectively). In particular, Fig. 8 shows that the shapes of the parameter variation obtained by Eq. 3 are more similar to those obtained by using the GRD model and may be in contrast with those obtained by using Eq. 2.

Finally, Fig. 9 shows the viscosity variation as a function of H_2O content (wt%) for all investigated samples at 730 and 1030 °C. These temperatures were chosen as corresponding to: a) the limiting temperature values close to the glass transition temperature (log η ~ 12) for anhydrous melts and b) a temperature approximating the maximum inferred eruptive temperature, calculated on the basis of phase

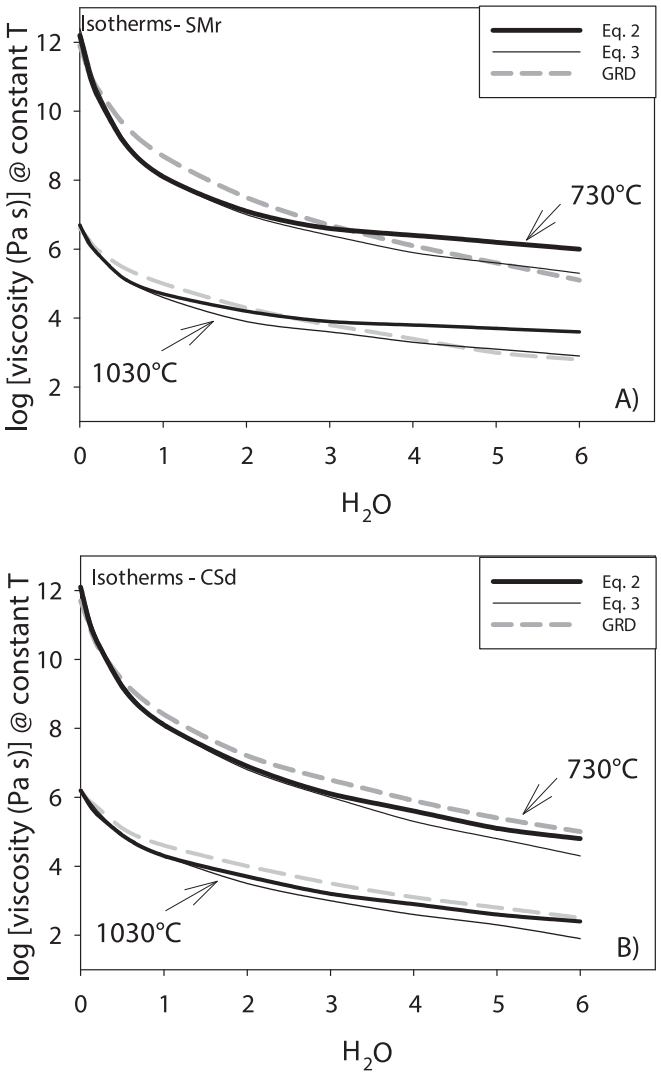

Fig. 9. Isothermal viscosity variation as a function of H_2O (wt%) as calculated at 730 °C (upper curves) and 1030 °C (lower curves) by using Eq. 2 (thick black lines) and Eq. 3 (thin black lines) and the GRD compositional model (grey dashed lines). The selected temperatures cover the entire eruption process until the end of the emplacement at the glass transition temperature (@ $\log\eta = 12$). Panel A) reports calculations on SMr sample while panel B) reports calculations for the CSd sample.

equilibria calculations (Polo et al., 2018a).

Thus, we assume that the temperature interval (730–1030 °C) corresponds to the entire interval from the beginning of the eruption to the end of the emplacement process. Fig. 9 shows that: i) for any given temperature, the viscosity decrease with the first 1–2 wt% dissolved H_2O being sharper than for any further addition; ii) the viscosity variation patterns with varying H_2O content for both SMr and CSd are, in general, similar; iii) the viscosities calculated for the two temperatures at anhydrous conditions differ substantially (5 orders of magnitude for SMr and 6 orders of magnitude for CSd) while the difference attenuates at the highest H_2O contents (~ 3 orders of magnitude for both samples).

Fig. 9A also shows that the viscosity variation as a function H_2O for the different model are in general comparable and only at H_2O content above ~2 wt%, the calculated viscosities using Eq. 2 for SMr sample slightly increase respect to those calculated by using Eq. 3 or the GRD model. The slight divergence is around 1 logunit at the highest H_2O is added to the melts.

Based on the analysis reported above, and by reminding that no objective physical meaning can be associated to any of the obtained empirical adjustable parameters, we conclude however that Eq. 3 appears to constitute a more appropriate form of equation to represent the viscosity and rheological parameters of the rhyolitic and dacitic magmas investigated here.

5.2. Comparison with previous results

To better compare our results with previous studies investigating the viscosity of volcanic products (representing either explosive or effusive eruptive events), we have compiled a list of samples already analyzed in the literature. In order to provide a consistent comparison, we have refitted the literature data according to Eqs. 1 and 3. Table 5 reports the values of the adjustable parameters of Eq. 3 for each considered compositions. The compositions are the same as analyzed by Giordano et al. (2009)(hence in order to obtain the corresponding volcanological details the reader should refer to that study) to which we have added the dataset provided by Di Genova et al. (2013) for Pantelleritic melts from Punta Spadillo (Pantelleria Island, Italy), having an eruptive temperature of 750 °C (e.g. Di Genova et al., 2013; Gioncada and Landi, 2010). These data were added as comparison to a low viscosity extreme for rhyolitic melts.

The calculated viscosity variations as a function of H_2O (wt%) at eruptive temperatures are reported in Fig. 10. Eruptive temperature for each composition was compiled from the literature by Giordano et al. (2009) and is reported in the figure caption. For the compositions measured here we have assumed an eruptive temperature of 1000 °C for both SMr and CSd. This value corresponds to an average value amongst those published by Polo et al. (2018a), which are based on geo-thermobarometric models.

Fig. 10 shows that, at their eruptive temperature, the viscosity of SMr and CSd samples is intermediate between those for which the eruptive style is prevalently explosive and those for which the eruptive style is prevalently effusive. At $H_2O = 2$ wt% (coherent with the water content estimated at depth and during the initial ascent stage for the CSd; Polo et al., 2018a), the viscosity of these magmas would be close to $10^{3.8}$ Pas. The same applies to the more mafic BCd sample, for which anhydrous viscosity was measured, and whose viscosity as a function of H_2O was calculated according to the GRD model (Fig. 10), considering an eruptive temperature of 1000 °C. Although, not unique, these values of temperature are significantly higher than those of most silicic products whereas the viscosity is significantly lower (ca. three orders of magnitude) than those of typical highly explosive rhyolites (e.g. Takeuchi, 2011; Polacci et al., 2004) and on the order of those of typical andesitic, teprhi-phonolitiic and phonotephritic flows of prevalently effusive eruptions. At the very low H_2O contents estimated for the SMr by Polo et al. (2018a) (0.5–1.0 wt%), the investigated rhyolitic magmas would have viscosities of the order of $\sim 10^{4.9}$–$10^{5.6}$ Pa s.

Fig. A.7 also shows the viscosity variation as a function of H_2O for all the compositions investigated at a unique temperature value of 1000 °C. This figure allows to understand what is the effect of H_2O on the different composition in a temperature-space.

5.3. Rheological properties of silicic magmas: Constraints on eruption and emplacement dynamics

Based on new experimental data, two new numerical expressions (Eq. 1 and Eq. 3) capable of accurately predicting the T and H_2O dependence of the liquid viscosity of both SMr and CSd have been

Table 5
Best fits parameters for Eq. 3 and Root Mean Square Errors of fits obtained by using Eq. 2*.

	B'_{VFT}	B''_{VFT}	C'_{VFT}	C''_{VFT}	RMSE (Eq. 3)	RMSE (Eq. 2)
Rhyolite (HPG8+HGG)	13143.0	-336.1	-223.9	523.2	0.23	0.23
+/-	180.3	98.8	19.7	23.1		
Trachyte (AMS_B1)	10381.9	-284.8	27.3	284.8	0.16	0.17
+/-	176.6	31.3	12.6	12.0		
Trachyte (IGC)	8978.0	16.2	16.4	465.6	0.22	0.20
+/-	155.4	55.2	14.5	16.5		
Trachyte (MNV)	10451.8	-452.0	59.0	243.4	0.09	0.10
+/-	79.7	23.3	7.66	7.74		
Phonolite (Teide)	10270.3	-68.9	-56.6	318.0	0.13	0.13
+/-	93.0	33.8	9.6	10.3		
Phonolite (Mercato)	10123.7	-332.9	37.3	271.0	0.22	0.21
+/-	151.4	49.1	12.9	18.2		
Pantellerite (PS)	10136.7	-162.5	-86.1	289.5	0.23	0.27*/0.25**
+/-	248.3	65.5	21.1	22.0		
Andesite	7792.0	-363.7	274.2	278.6	0.15	0.15
+/-	59.37	19.83	5.62	5.56		
Tephri-Phonolite (1631W)	8218.6	-245.6	150.4	284.7	0.15	0.16
+/-	127.3	36.8	11.8	11.0		
Phono-Tefrite (1631G)	8413.5	-285.7	133.1	306.8	0.18	0.19
+/-	150.8	62.5	16.7	15.8		
Trachybasalt (ETNA)	5703.4	54.2	319.9	299.9	0.22	0.20
+/-	142.2	67.7	14.2	15.4		
Tefrite (1906)	6080.2	-37.7	311.4	258.9	0.18	0.16
+/-	90.9	40.4	9.7	11.4		
Basalt (Stromboli)	6164.9	-270.2	358.3	203.2	0.23	0.21
+/-	80.2	31.3	8.6	10.9		
Rhyolite (SMr)	10064.9	-176.0	34.6	375.3	0.12	0.11
+/-	74.01	18.89	6.95	7.44		
Dacite (CSd)	9213.04	-338.14	148.49	301.27	0.14	0.14
+/-	81.31	28.64	8.33	8.50		
Dacite (BCd)	9081.6		353.1		0.01	0.01
+/-	54.45		7.27			

* Giordano et al. (2009); ** Di Genova et al. (2013)

provided here. These expressions were shown to provide viscosity variations similar to those obtained by employing the GRD model (Giordano et al., 2008). For that reason, our study may corroborate the conclusions of Polo et al. (2018a, 2018b) which were based on the GRD model. They calculated the P-T-H_2O conditions likely acting during the pre, *syn*- and post-eruptive phases of Palmas-type degassed magmas and volcanic products and proposed that, given the high eruption temperatures the investigated silicic magmas had low viscosities. They suggested these viscosities to be characteristic of low viscosity lava flows or lava-like rheomorphic ignimbrite flows, potentially deriving from low intensity explosive eruptions.

The experimental results obtained here indicate that the crystal-poor (<10 vol%) Palmas-type dacitic and rhyolitic magmas, inferred to have ascended at high temperatures (~1000 °C) and low H_2O content (<2 wt %) (Polo et al., 2018a; Simões et al., 2018b), had effective viscosity values between 10^4 and 10^6 Pa s (Fig. 10). In the case of the rhyolite (SMr), the remarkably low estimated H_2O contents (<1 wt%) would result in a viscosity up to two orders of magnitude higher than the two dacites (CSd and BCd), a value that, due to the high estimated eruptive temperature for silicic products, could still be lower than those typical for rhyolitic eruptions. In all cases, viscosity values at the highest H_2O content are typical of highly mobile andesitic and tephri-phonolitic lava flows. Fragmentation of these magmas is suppressed even for the highest discharge rates; fragmentation would require, according to the fragile fragmentation criterion (e.g. Dingwell, 1996; Papale, 1999), strain-rates higher than 10^3 s^{-1} which are unlikely also for large eruption. Analogously, the maximum viscosities at low H_2O content for both SMr and CSd are close to, but still lower with respect to those (>10^7 Pa s) necessary to cross the glass transition and provide a brittle failure of the ascending magmas (e.g. Papale, 1999; Polacci et al., 2004). In addition, the low H_2O content will not allow an as efficient and fast ascent in the conduit capable to determine fragmentation Consistent with the viscosity calculations provided by Polo et al. (2018a), who used the GRD model, our results confirm at first approximation, the conclusions discussed by Polo et al. (2018 a, b), which demonstrate that the Eocretacic volcanism that also occurred in the Gramado Xavier region was likely capable of forming lava flows.

Nonetheless, we cannot disregard the hypothesis that explosive volcanism also occurred in the area, as observed by previous authors (e.g. Guimaraes et al., 2018a,b, 2019). In fact "strain-induced" fragmentation is possible for low residual melt viscosity if unusual conditions, providing for either very high viscosity of the magmatic mixture and/or very high strain rate, occur during an eruption.

One possibility to increase viscosity of low viscosity melts is by addition of significant proportions of crystals. A possible, but so far undetected, nanolite crystallization could bring the investigated magmas to behave brittle and fragment as a consequence of the crossing of the glass transition interval (e.g. Papale, 1999; Dingwell, 1996). This last issue, that is the effect of nanolite crystallization on eruption dynamics, is a topic of particular relevance which has to be further investigated and comprehended in volcanology. In fact, volcanic products may contain nanolites, whose crystallization can play a crucial role in determining the effective physical properties of magmas and volcanic products, and therefore may substantially affect the eruption dynamics of both effusive (e.g. Stevenson et al., 1996) and explosive (Di Genova et al., 2018) episodes. As shown by previous studies the degree of

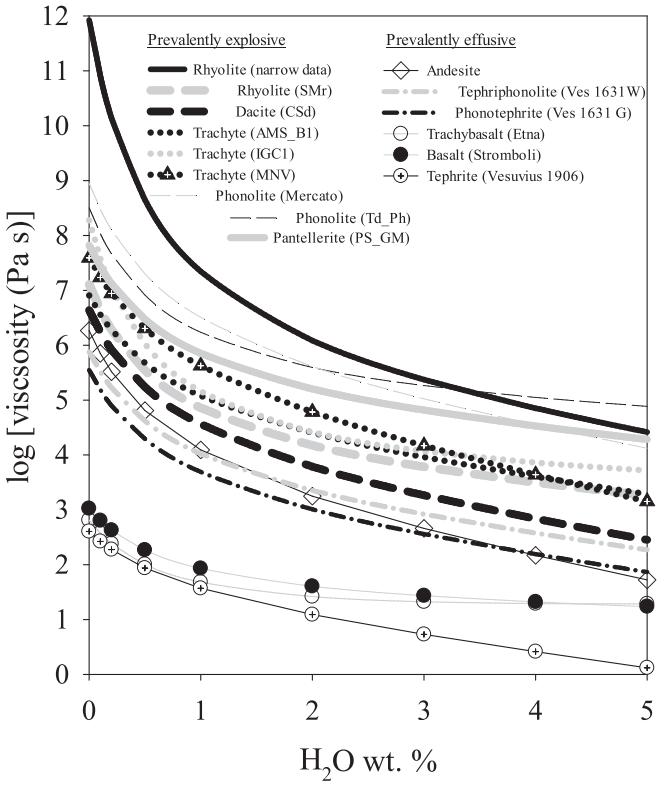

Fig. 10. *Calculated viscosity vs H2O variation at eruptive temperatures. The eruptive temperatures are taken from* Giordano et al. *(2009) and references therein and* Polo et al. *(2018a). Eruptive temperatures of: 830 °C for the "narrow database" considered in the model from* Ardia et al. *(2008); 785 °C for the Mercato phonolite; 750 °C for the Punta Spadilla Pantellerite melt (*Di Genova et al., 2013*; Gioncada and Landi, 2010); 1100 °C for the phono-tephrite of the 1906 eruption; 977 °C for the tephri-phonolite of the 1631_W_GM Vesuvius eruption; 890, 900 and 945 °C for the trachytic melts of Monte Nuovo (MNV), Ignimbrite Campana (IGC) and Agnano Monte Spina (AMSB1), respectively (Piochi* et al.*, 2008); 775 °C for the Phonolite from Montana Blanca eurption; 1125 _C for the Etna trachybasalt and 1150 °C for the Stromboli (HK) basalt. Temperature of 1000 °C has been taken for both the SMr and CSd as an intermediate temperature estimates for these kinds of magmas (*Polo et al., 2018a*). Finally, calculated viscosities at T = 1000 °C for the Fe-rich BCd have been added to the graph. An apparent correlation between viscosity and eruptive style emerges, where higher viscosity products also produce typical explosive activity (plinian and subplinian), lower viscosity products produce effusive, strombolian or fire fountaining activity. Intermediate products such as the andesite (diamonds) and both the tephriphonolites and phono-tephrites (black and grey crosses) could produce eruptions of both mildly explosive to effusive products.*

nanolitization is complex to retrieve, but apparently less complex is the task of determining what is the effect of the presence of nanolites on the physical properties (Di Genova et al., 2018). The natural re-melted and quenched products used for experimentation do not contain nanolites as verified by Raman spectroscopy in previous investigations (e.g. Giordano et al., 2019; González-García et al., 2020). In fact, in these previous works on a substantial number of anhydrous samples which were re-melted at high temperature and then quenched (e.g. González-García et al., 2020– this issue) we did not observe the presence of nanolites. The most curious case is some of the glasses we have investigated here which, although re-melted and fast quenched at room temperature, in all cases, but one, gave origin to the formation of nanolites.

So, the questions that raise spontaneous are: "is this a process frequently occurring in nature? If yes, in which magmatic/volcanic context?" "Does nanolitization occur in pre-, *syn-* or post-eruptive stages? Does the presence of natural dissolved volatiles prevent/favor to some extent the formation of nanolites during certain magmatic, eruptive or post-eruptive stages? What are indeed the volcanological consequences of the occurrence of this process in nature? Many of these question are still unanswered and need further investigation, on volatile-bearing melts. In fact, we have no idea if nano-crystallization, if occurring in natural melts, will indeed increase (by addition of crystals) or decrease (via the enrichment of residual melt in volatiles) the viscosity of natural melts. The question remains on why, amongst all the previously investigated samples, re-melted at high temperature and rapidly quenched rapidly, only those investigated here gave origin to nano-crystals? These melts are enriched in Fe—Ti component which may have enhanced syn-eruptive nanolitization. The source of Fe—Ti enrichment remains uncertain.

On the other hand, the above-mentioned possibility to increase the strain rate may include external forcing such as a rapid depressurization of the magmatic system through, for instance, edifice collapse or strong earthquakes, or the quenching of the stored magma via magma-water interaction. Related to this, and in relation with the low viscosity silicic magmas investigated here we may invoke the occurrence of sudden large decompression of the storage system feeding PMP eruptions, which would provide support to the hypotheses of the occurrence of explosive eruptions. From a volcanological perspective, at present, due to the lack of evidence of geophysical studies of the deposits which might associated them to large volcanic structures, such as calderas (like those described in the neighbour PEMP regions from Namibia (Etendeka) and Uruguay (Paranà)), large fissure structures, such as that of remarkable size (15 km in diameter) shown by previous authors (e.g. Fig. 4 in Polo et al., 2018b; Lima et al., 2012), have to be considered as the best candidates for future field work.

6. Conclusions

This paper provides new equations describing the temperature and H_2O content dependence of the pure liquid viscosities of rhyolitic and dacitic magmas associated with representative volcanic products of the Caxias do Sul and Santa Maria eruptive sequences. The new parameterizations (Eq. 3) provide similar values to those obtained from the GRD model (Giordano et al., 2008), but different from previous equations (Eq. 2) which do not accurately constrain the H_2O content variation of single VFT parameters. The role of the small amount of nanolites detected by Raman spectroscopy in the post-run samples measured here are suggested to have a minor influence on viscosity measurements, but further investigation is required.

In agreement with previous work, our investigation reported that the Paraná Palmas-type silicic volcanism is characterized by high pre-eruptive temperatures (>950 °C) and by the emission of large volumes (~20.000 km^3) degassed products (< 2 wt% H_2O) as manifested by others LIP and hotspot tectonic settings. This kind of eruptions are rare on Earth as they occur with an average frequency of ca 20 Ma giving origin to explosive and effusive catastrophic super eruptions (with magnitude > M8, see Bryan et al., 2010) and are, consequently, very complex to understand. The work provided here provides one more little step ahead toward the comprehension of the complex eruptive scenario at the origin of the volcanism of the PMP. The expressions provided here constitute a first step forward toward the development of numerical modelling studies that, by accounting for the established contour conditions (e.g. geometrical constraints of the feeding system; physico-chemical characterization of rising magmas), will allow testing the

still debated eruptive scenarios for the magmatism of the southern part of the Parana-Etendeka Magmatic Province.

Indeed, further fieldwork investigation and sample analyses are required to lead to a more complete understanding of volcanic scenario at the moment of the eruption of the PMP. Contemporaneously the development of new experimental volcanology and petrology studies, together with the employment of numerical simulations will be necessary.

Declaration of Competing Interest

The authors declare that they have no known competing financial interests or personal relationships that could have appeared to influence the work reported in this paper.

Acknowledgements

Financial support for this work was given by Fapesp (ThematicProject 2012/06082-6). LAP acknowledges a post-Doctoral scholarship by FAPESP (proc: 2017/15540-1). DG visits and research at the Universidade de São Paulo (2015-2017) are financed by a PVE (Pesquisador Visitante Especial) Project funded by CAPES (proc:88881.068169/2014-01; PVE: DG; Responsible: VAJ) within the framework of CSF program, Brazil. LFG was supported by a CNPq PhD fellowship (No. 142084/2015-8) and CAPES PDSE fellowship (No. 88881.134384/ 2016-01). We acknowledge the financial support from DAAD Project 57389574 "Large Igneous province Paraná-Etendeka". SK acknowledges the support of a H2020 Marie Skłodowska-Curie fellowship DYNAVOLC – No.795044. AV and CR acknowledge the Grant of Excellence Departments, MIUR-Italy (ARTICOLO 1, COMMI 314 - 337 LEGGE 232/2016). DGG was supported by a postdoctoral fellowship cofounded by the University of Turin and LMU Munich. AA was funded by the German Science Foundation (DFG NO378/12). Melanie Kaliwoda is acknowledged for assistance during Micro-Raman analyses in Munich. DBD acknowledges the support of ERC-ADV-2018 Grant 834225 (EAVESDROP). We are grateful to two anonymous reviewers for their revision which helped us to improve the quality of this manuscript.

Appendix A. Experimental techniques

A.0 Analytical methods

The major element compositions of both natural glass matrix and remelted total rock samples were obtained using a Cameca SX100 electron probe microanalyzer (EPMA) at the Department for Earth and Environmental Sciences (LMU Munich, Germany). Operating conditions were an acceleration voltage of 15 kV and beam current of 4 nA, using a defocused 10-μm beam in order to minimize alkali loss. Albite, periclase, apatite, wollastonite, bustamite, Fe_2O_3 and ilmenite were used as standards. Standard deviations were lower than 2.5% for all analyzed elements. Precision and accuracy were checked by analysing the reference glasses VG-2 (basalt) and VG-568 (rhyolite) (Jarosewich et al., 1980; Helz et al., 2014) at the start of each analytical session. No significant alkali loss was observed relative to tabulated values of standards.

A.1. High-T viscosity determination

Superliquidus viscosity measurements, between $10^{2.1}$ and $10^{4.7}$ Pa s, were obtained using the concentric cylinder system and method described in Dingwell (1996). These were performed on the anhydrous samples, after homogenization, in a Deltech furnace using a Brookfield DVIII (full-scale torque = 0.7187 mNm) viscometer head and a $Pt_{80}Rh_{20}$ spindle (e.g., Dingwell and Virgo, 1988). About 65 g batches of each sample were loaded separately into the Deltech furnace and melted at 1300 to 1600 °C (depending on composition) and stirred for several hours. After inspection of the stirring spindle revealed that the melts were physically homogeneous, the melt viscosities were measured. After the measurement, the melts were removed from the furnace and quenched in air within the measurement crucible. The measuring stage consisted of determining the viscosity in steps of decreasing temperature with a final measurement again at the highest temperature to check for any drift during each measurement series. The viscosity standard, DGG-1, was used to calibrate the system and the viscosities are accurate to within 5%. Cylinders, of a 3–5 mm in diameter, were cored from the glasses and cut into disks 2 to 3 mm thick which were finally doubly polished, dried and stored in a desiccator until further use (e.g. Raman spectroscopy; Micropenetration § A.2.).

A.2. Low-T viscosity determination

Micropenetration measurements for both dry and water-bearing samples in a viscosity interval between $10^{9.49}$ and $10^{11.25}$ Pa s were performed using a vertical push-rod Setaram Setsys (EVPLab, Department of Science, Roma Tre University) dilatometer (e.g., Hess and Dingwell, 1996; Giordano et al., 2005, Giordano et al., 2008, Di Genova et al., 2014, and reference therein). The system was calibrated with the standard glass DGG-1 of the Physikalisch-Technische Bundesanstalt (PTB). This method is based on the determination of the rate at which a hemispherical Ir-indenter penetrates under a fixed load into a melt surface. The absolute shear viscosity is determined via the following equation:

$$\eta = \frac{0.1875 \cdot P \cdot t}{r^{0.5} d^{1.5}} \tag{A.1}$$

(Pocklington, 1940; Tobolsky and Taylor, 1963) where P is the applied force, r is the radius of the hemisphere, t is the penetration time and d is the indentation distance. This provides an accurate viscosity value if the indentation distance is less than 150–200 μm. One of the main advantages of this technique is the small amount of material (< 10 mg) required to perform a measurement. The samples were heated in the dilatometer at a constant rate of 25 °C/min to a temperature around 100 °C below the temperature at which the measurement was performed. The samples were then heated at a rate of 5 °C/min to the target temperature, where they were allowed to relax during an isothermal dwell of about 10–15 min. During the entire heat treatment, the indenter (radius $r = 1$ mm) sits on the sample surface and an upwards force balancing the indenter weight is applied (i.e., zero weight

conditions). At the end of the dwell time, a downward force (0.98 N) is applied to let the indenter penetrate the sample and the viscosity measurement was stopped, once a stable viscosity values was reached. The error in the viscosity measurements was estimated equal to ±0.1 log Pa s. Each measurement was performed at isothermal conditions using a new sample to avoid sequential water loss. The geometry of the indentation - time relation resulting from the measurements enable evaluation of whether exsolution or other kinetics processes affecting the viscosity measurement occurred during the run. Measurements which showed evidence of these processes were not used (Giordano et al., 2009). The data obtained using this technique are reported in Tables 3 for the anhydrous and water-bearing samples respectively.

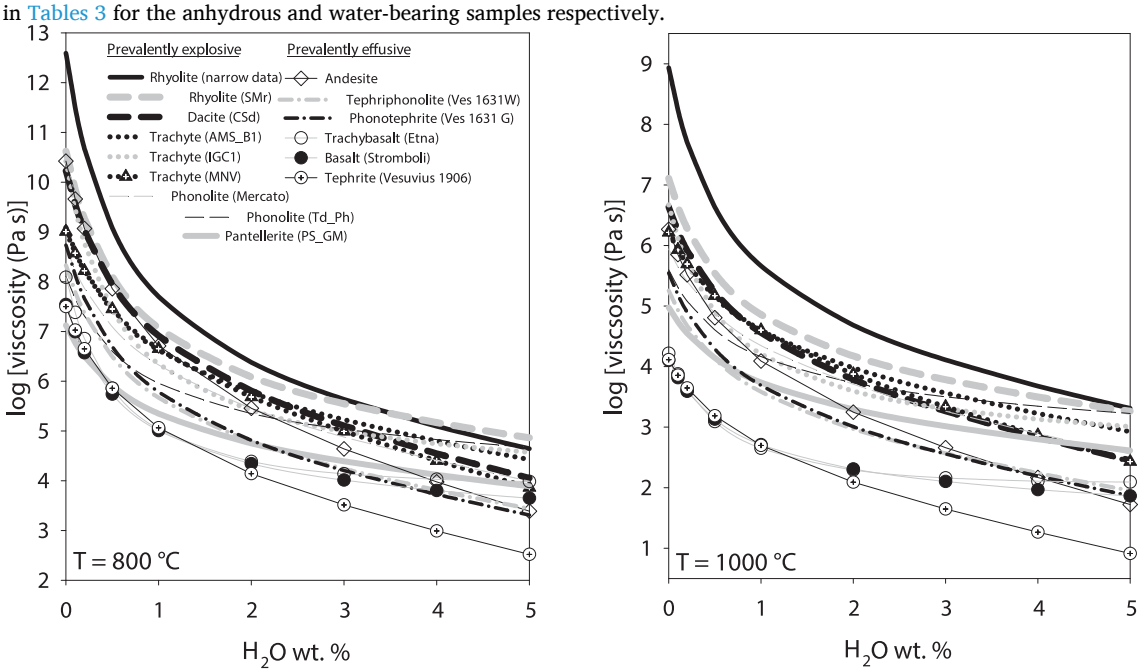

Fig. A.2. Example of micropenetration viscometry for sample GX07–1 run at 660.1 °C, showing temporal variation of (left) temperature, (center) indentation, and (right) calculated viscosity according to Eq. (A.1).

A.3. Hydration experiment in an Internally Heated Pressure Vessell (IHPV)

For the hydration experiments, the RS74 and GX07 samples material was crushed with a steel mortar and sieved to grain sizes of <500 μm. $Au_{80}Pd_{20}$ capsules (OD:5.4 mm; ID: 5.0 mm) were chosen to avoid Fe loss into the capsule material (Berndt et al. 2002). Before capsule closure, these were cleaned with ethanol and annealed at 800 °C for 8 h. For hydration of rhyolite and dacite, 20 and 25 mm long tubes were crimped and welded to a three-sided star at the bottom. The tubes were then stepwise filled with sample material, which was densified with a steel piston. The required amount of H_2O was then added to the sample material with a digitally controlled Eppendorf micropipette. After the filling of the capsules with the required proportions of H_2O and sample powders, the upper parts of the capsules were once more crimped to a three-sided star and welded shut. To check for possible H_2O leakage, the capsules were heated in a compartment dryer (110 °C) for at least 1 h and re-weighed to detect possible H_2O loss. To exclude leakage during pressure induced capsule deformation, the capsules were re-weighed after a compression at 100 MPa and ambient T and again after heating in the dryer.

Hydration runs were conducted in an internally heated argon pressure vessel (IHPV) at intrinsic oxygen fugacities of ΔlogFMQ between ~ + 2.5 to – 3.5, depending on H_2O content. At 2 kbar the samples were heated with 25 K/min to 1250 °C. After run time of 24 h the capsules were quenched isobarically at ~16 K/s by shutting off the furnace (Allabar et al., 2020). This cooling rate is slow enough to prevent the sample from cooling induced tension crack formation. After the experiments, the capsules were re-weighed to check for possible leakage. Ten (5 + 5) hydrous syntheses were performed for the GX07 and the RS74 sample, respectively. Water-bearing samples, containing up to 5.27 wt%, have been obtained (Table 2).

A.4. Karl-Fischer Titration

- The homogeneity and the absolute water contents of the hydrous glass samples GX07 and RS74 were checked by Karl Fischer Titration (KFT) at the Institute of Mineralogy, Leibniz University, Hannover, using the methods described by Behrens et al. (1996) and Nowak and Behrens (1997). Measured water contents were corrected for the unextracted water content as reported by previous authors (Behrens and Stuke, 2003; Leschik et al., 2004). Uluguru muscovite (4.15 ± 0.10 wt% H_2O) was used as reference material. The considered water contents are reported in Table 2 with the technique used for the quantification. In order to provide viscosity models of the investigated compositions we have taken the average of two measurements, when available (Table 2).

A.5. MicroRaman spectroscopy

- Micro-Raman analyses were performed on glass disks of GX07 and RS74 samples in order to establish the homogeneous distribution of dissolved water of the hydrothermal syntheses as well as to detect the possible occurrence of crystals. Raman spectroscopy was carried out at the for Earth

and Environmental Sciences, LMU Munich, using a confocal integrated micro−/macro-Raman spectrometer Horiba Jobin Yvon XploRa ONE equipped with edge filters and a Peltier-cooled Charge Coupled Device (CCD) detector, managed by the Mineralogical State Collection (MSM) of Munich. An excitation line of 532 nm wavelength (2ω-Nd:YAG laser) was used, with a slit of 200 μm and a grating of 1800 grooves per millimeter. Each spectrum was collected in confocal setting with a hole of 300 μm, and the laser was focused on the sample using an objective of 100×. Exposure times were of 10 × 30 s. An attenuation filter of 50% was used, resulting in a laser power of 5.5 ± 0.1 mW at the sample surface. The calibration of the instrument was checked before each analytical session using the 521-cm^{-1} silicon band, with accuracy and precision in the order of 1 cm^{-1}. Water content homogeneity is estimated by verifying that the ca 3500 cm^{-1} peak would not substantially change as measured in different areas of the same samples. As put in evidence by Giordano et al. (2019) (Fig. S1) uncertainties associated to Raman peak intensity and calculated parameters is in the order of 5% relative error for those samples having lower LW measured values and smaller than that value for samples having high LW values.

A.6. X-Ray Diffraction analysis

- As reported in the main text both anhydrous and hydrated samples were quenched rapidly after concentric cylinder experiments and hydrothermal syntheses and prepared in order to check for the potential presence of micro- or nano-crystals via X-ray diffraction. Powder XRD analyses were done by using a Philips X'Pert diffractometer at the Department for Earth and Environmental Sciences, LMU Munich. The samples were ground in an agate mortar, placed on a silicon zero-background sample holder and measured with Cu-Kα radiation in a 2θ range between 10 and 85°. Step size was 0.02° with a measurement time of 1 s per step. The predominant absence (or non-quantifiable height) of peaks in the XRD spectra (Fig. A.6.1., A.6.2) indicate that a negligible amount of Fe-oxide nano-crystals (<1.5 wt%; ca 1 vol%) is present in the measured glasses, except in the natural sample. As a consequence, in our investigation we assumed that the influence of the physical presence of nanolites on the measured high temperature and low temperature anhydrous and hydrous melt viscosity was negligible.

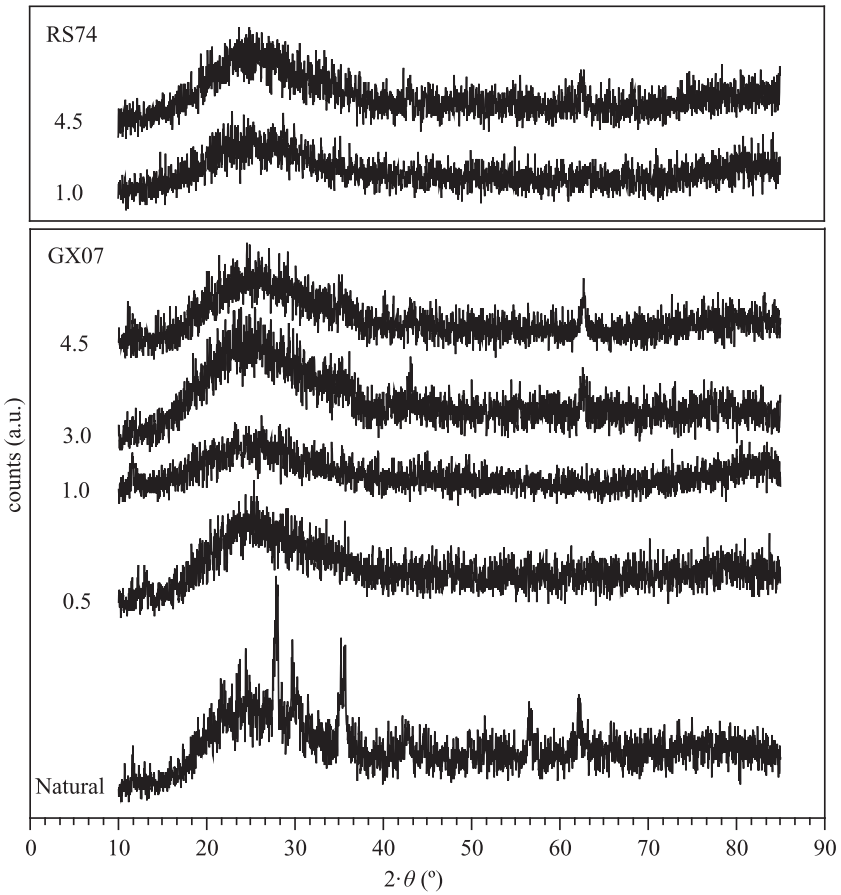

Fig. A.6. X-ray powder diffraction spectra of RS74 and GX07 glasses. The RS74 panels represent the powder XRD pattern of sample (from bottom to top) RS74_1 and RS74_3. The GX07 panels are associated with (from top to bottom) GX07_4.5; GX07_3.0, GX07_1.0_GX07_0.5 and natural, for which H_2O contents are given in Table 2. The hump at 2 θ centered around 25° in all samples is derived from the amorphous silicate matrix. The other peaks, only visible in the natural sample, belong to a spinel phase (magnetite, Fe—Ti oxide or Mg-ferrite) or plagioclase (labradorite, bytownite) minerals. So far it concerns with the hydrous glasses only very tiny peaks are observed belonging to a spinel phase.

A.7. Comparison of viscosity as a function of water at constant temperatures

See Fig A.7

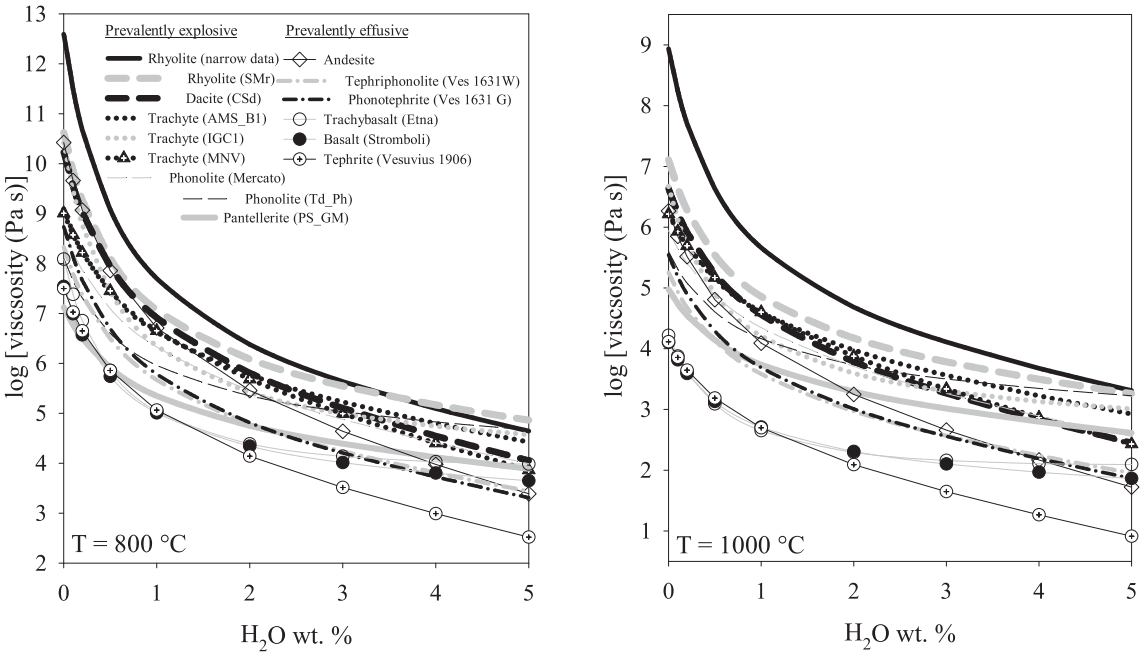

Fig. A.7. Isothermal viscosity variation of the samples investigated in the present study as calculated using Eq. 3. Symbols are as in Fig. 10. The figure puts in evidence that a more relevant viscosity decrease is expected for more polymerised compositions, such as those of the "narrow database" of Ardia et al. (2008). For all compositions, a proportionally larger viscosity decrease is observed when small amounts of water are incorporated into the melt. Largely, rhyolitic melts are more viscous than trachytes which are more viscous than phonolites, tephri-phonolites and basalts. This trend is particularly evident at low H_2O contents than al high H_2O content where melt viscosity tends to cross-over (Giordano et al., 2009). Particular behaviour is shown by iron-rich rhyolites (e.g. SMr and PS_GM) which show a lower effect of the addition of H_2O in decreasing the viscosity which starts from about 1/1.5 wt% H_2O. In particular, the pantellerite from Punta Spadilla which, al low H_2O content, has viscosity similar to those of the most depolymerized melts (e.g. tephriphonolite, basalts and teprhites), at the highest H_2O contents assumes viscosity values comparable with the dacitic and trachytic compositions.

References

Allabar, A., Dobson, K.J., Bauer, C.C., Nowak, M., 2020. Vesicle shrinkage in hydrous phonolitic melt during cooling. Contrib. Min. Pet. 175, 21. https://doi.org/10.1007/s00410-020-1658-3.

Andrews, G.D.M., Branney, M.J., 2005. Folds, fabrics, and kinematic criteria in rheomorphic ignimbrites of the Snake River Plain, Idaho: Insights into emplacement and flow. Geol. Soc. Am. Field Guide 6, 311–328.

Andrews, G.D.M., Branney, M.J., 2011. Emplacement and rheomorphic deformation of a large, lava-like rhyolitic ignimbrite: Grey's Landing, southern Idaho. Geol. Soc. Am. Bull. 123, 725–743.

Andrews, G.D.M., Branney, M.J., Bonnichsen, B., McCurry, M., 2008. Rhyolitic ignimbrites in the Rogerson Graben, southern Snake River Plain volcanic province: volcanic stratigraphy, eruption history and basin evolution. Bull. Volcanol. 70, 269–291.

Angell, C.A., 1985. In: Ngai, K.L., Wright, G.B. (Eds.), Relaxation in Complex Systems. U. S. Department of Commerce National Technical Information Service, Springfield, VA, pp. 3–11.

Ardia, P., Giordano, D., Schmidt, M.W., 2008. A model for the viscosity of rhyolite as a function of H_2O-content and pressure: a calibration based on centrifuge piston cylinder experiments. Geochim. Cosmochim. Acta 72, 6103–6123.

Behrens, H., Stuke, A., 2003. Quantification of H_2O contents in silicate glasses using IR spectroscopy - a calibration based on hydrous glasses analyzed by Karl-Fischer titration. Glas. Sci. Technol. 76, 176–189.

Behrens, H., Romano, C., Nowak, M., Holtz, F., Dingwell, D.B., 1996. Near-infrared spectroscopic determination of water species in glasses of system $MAlSi_3O_8$ (M=Li, Na, K): an interlaboratory study. Chem. Geol. 128, 41–63.

Bellieni, G., Comin-Chiaramonti, P, Marques, L.S, Melfi, A.J., Nardy, A.J.R., Papatrechas, C., Piccirillo, E.M., Roisemberg, A., Stolfa, D., 1986. Petrogenetic Aspects of Acid and Basaltic Lavas from the Paraná Plateau (Brazil): Geological, Mineralogical and Petrochemical Relationships. J. Petrol. 27(4), 915–944.

Branney, M.J., Barry, T.L., Godchaux, M., 2004. Sheathfolds in rheomorphic ignimbrites. Bull. Volcanol. 66, 485–491. https://doi.org/10.1007/s00445-003-0332-8.

Bryan, S.E., Peate, I.U., Peate, D.W., Self, S., Jerram, D.A., Mawby, M.R., Marsh, J.S., Miller, J.A., 2010. The largest volcanic eruptions on Earth. Earth-Sci. Rev. 102 (3), 207–229.

Cañón-Tapia, E., Raposo, M.I.B., 2018. Anisotropy of magnetic susceptibility of silicic rocks from quarries in the vicinity of São Marcos, Rio Grande do Sul, South Brazil: Implications for emplacement mechanisms. J. Volcanol. Geotherm. Res. 355, 165–180. https://doi.org/10.1016/j.jvolgeores.2017.07.018.

Cassidy, M., Manga, M., Cashman, K., Bachmann, O., 2018. Controls on explosive-effusive volcanic eruption styles. Nature Comm. 9, 2839. https://doi.org/10.1038/s41467-018-.05293-3.

Castro, J.M., Schipper, C.I., Mueller, S.P., Militzer, A.S., Amigo, A., Parejas, C.S., Jacob, D., 2013. Storage and eruption of near-liquidus rhyolite magma at Cordón Caulle. Chile. Bull. Volcanol. 75 (4), 1–17.

De Campos, C.P., Guimarães, L.F., Lima, E.F., Janasi, V.A., Giordano, D., Dingwell, D.B., 2016. Chaotic flow and fragmentation patterns in the acidic feeder system from the Paraná-Etendeka large Igneous Province. Goldschmidt Conference Abstracts, 2413.

De Faria, D.L.A., Venancio Silva, S., De Oliveira, M.T., 1997. Raman microspectroscopy of some iron oxides and oxyhydroxides. J. Raman Spectrosc. 28, 873–878.

Di Genova, D., Romano, C., Hess, K.U., Vona, A., Poe, B.T., Giordano, D., Dingwell, D.B., Behrens, H., 2013. The rheology of peralkaline rhyolites from Pantelleria Island. J. Volcanol. Geoth. Res. 249, 201–216.

Stevenson, R.J., Dingwell, D.B., Webb, S.L., Sharp, T.G., 2014. Heat capacity configurational heat capacity and fragility of hydrous magmas. Geochim. Cosmochim. Acta 142, 314–333.

Di Genova, D., Kolzenburg, S., Wiesmaier, S., Dallanave, E., Neuville, D.R., Hess, K.-U., Dingwell, D.B., 2017. A chemical tipping point governing mobilization and eruption style of rhyolitic magma. Nature 552, 235–238. https://doi.org/10.1038/nature24488.

Di Genova, D., Caracciolo, A., Kolzenburg, S., 2018. Measuring the degree of "nanotilization" of volcanic glasses: Understanding syn-eruptive processes recorded in melt inclusions. Lithos 318–319, 209–218. https://doi.org/10.1016/j.lithos.2018.08.011.

Dingwell, D.B., 1996. Volcanic dilemma: Flow or blow? Science 273, 1054–1055.

Dingwell, D.B., Romano, C., Hess, K.-U., 1996. The effect of water on the viscosity of a haplogranitic melt under P-T-X conditions relevant to silic volcanism. Contrib. Mineral. Petrol. 124, 19–28.

Ernesto, M., Raposo, M.I.B., Marques, L.S., Renne, P.R., Diogo, L.A., de Min, A., 1999. Paleomagnetism, geochemistry and $^{40}Ar/^{39}Ar$ dating of the North-eastern Paraná Magmatic Province: tectonic implications. J. Geodyn. 28 (4), 321–340. https://doi.org/10.1016/S0264-3707(99)00013-7.

Florisbal, L.M., Heaman, L.M., Janasi, V.A., Bitencourt, M.F., 2014. Tectonic significance of the Florianópolis Dyke Swarm, Paraná-Etendeka Magmatic Province: a reappraisal based on precise U-Pb dating. J. Volcanol. Geotherm. Res. 289, 140–150. https://doi.org/10.1016/j.jvolgeores.2014.11.007.

Frank, H.T., Gomes, M.E.B., Formoso, M.L.L., 2009. Review of the areal extent and the volume of the Serra Geral Formation, Paraná Basin, South America. Pesqui. Geoc. 36 (1), 49–57.

Fulcher, G.S., 1925. Analysis of recent measurements of the viscosity of glasses. J. Am. Ceram. Soc. 8, 339–355.

Garland, F., Hawkesworth, C.J., Mantovani, M.S.M., 1995. Description and petrogenesis of the Paraná rhyolites, southern Brazil. J. Petrol. 36, 1127–1193.

Gioncada, A., Landi, P., 2010. The pre-eruptive volatile contents of recent basaltic and pantelleritic magmas at Pantelleria (Italy). J. Volcanol. Geoth. Res. 189, 191–201.

Giordano, D., Russell, J.K., 2007. A rheological model for glass forming silicate melts in the systems CAS, MAS. MCAS. J. Phys.: Condes. Matter 19, 205148.

Giordano, D., Romano, C., Papale, P., Dingwell, D.B., 2004. The viscosity of trachytes, and comparison with basalts, phonolites, and rhyolites. Chem. Geol. 213, 49–61.

Giordano, D., Nichols, A.R.L., Dingwell, D.B., 2005. Glass transition temperatures of natural hydrous melts: a relationship with shear viscosity and implications for the welding process. J. Volcanol. Geoth. Res. 142, 105–118.

Giordano, D., Russell, J.K., Dingwell, D.B., 2008. Viscosity of magmatic liquids: a model. Earth Planet. Sc. Lett. 271 (1), 123–134.

Giordano, D., Ardia, P., Romano, C., Dingwell, D.B., Di Muro, A., Schmidt, M.W., Mangiacapra, A., Hess, K.-U., 2009. The rheological evolution of alkaline Vesuvius magmas and comparison with alkaline series from the Phlegrean Fields, Etna. Stromboli and Teide. Geochim. Cosmochim. Acta 73, 6613–6630.

Giordano, D., González-García, D., Russell, J.K., Raneri, S., Bersani, D., Fornasini, L., Di Genova, D., Ferrando, S., Kaliwoda, M., Lottici, P.P., Smit, M., Dingwell, D.B., 2019. A calibrated database of Raman spectra for natural silicate glasses: implications for modelling melt physical properties. J. Raman Spectrosc. 51, 1822–1838.

Gonnermann, H.M., Manga, M., 2007. The Fluid Mechanics Inside a Volcano. Annu. Rev. Fluid Mech. 39, 321–356. https://doi.org/10.1146/annurev.fluid.39.050905.110207.

González-García, D., Giordano, D., Russell, J.K., Dingwell, D.B., 2020. A Raman spectroscopic tool to estimate chemical composition of natural volcanic glasses. Chem. Geol. 556, 119819. https://doi.org/10.1016/j.chemgeo.2020.119819.

Guimarães, L.F., Raposo, M.I.B., Janasi, V.A., Cañón-Tapia, E., Polo, L.A., 2018a. An AMS study of different silicic units from the southern Paraná-Etendeka Magmatic Province in Brazil: implications for the identification of flow directions and local feeding. J. Volcanol. Geotherm. 355, 304–318. https://doi.org/10.1016/j.jvolgeores.2017.11.014.

Guimarães, L.F., De Campos, C.P., Janasi, V.A., Lima, E.F., Dingwell, D.B., 2018b. Flow and fragmentation patterns in the silicic feeder system and related deposits in the Paraná-Etendeka Magmatic Province, São Marcos, South Brazil. J. Volcanol. Geoth. Res. 358, 149–164. https://doi.org/10.1016/j.jvolgeores.2018.03.021.

Guimarães, L.F., Hornby, A., Kueppers, U., Alves, A., Janasi, V.A., Dingwell, D.B., 2019. Generation of block-and-ash flows at the onset of silicic volcanism in the Paraná Magmatic Province (Brazil): evidence from photoanalysis of Caxias do Sul breccias. B. Volcanol. 81, 65. https://doi.org/10.1007/s00445-019-1332-7.

Helz, R.L., Clague D.A., Mastin L.G., Rose T.R. (2014). Electron microprobe analyses of glasses from Kilauea tephra units, Kilauea Volcano, Hawaii. Open-File report USGS doi: 10.3133/ofr2014090.

Henry, C.D., Wolff, J.A., 1992. Distinguishing strongly rheomorphic tuffs from extensive silicic lavas. B. Volcanol. 54, 171–186. https://doi.org/10.1007/BF00278387.

Hess, K.-U., Dingwell, D.B., 1996. Viscosities of hydrous leucogranitic melts: a non-Arrhenian model. Am. Mineral. 81, 1297–1300.

Janasi, V.A., de Freitas, V.A., Heaman, L.H., 2011. The onset of flood basalt volcanism, Northern Paraná Basin, Brazil: a precise U-Pb baddeleyite/zircon age for a Chapecó-type dacite. Earth Planet. Sci. Lett. 302 (1–2), 147–153.

E. JAROSEWICH J.A. NELEN Julie A. NORBERG (1980). Reference Samples for Electron Microprobe Analysis. Geostandards Newsletter https://doi.org/10.1111/j.1751-908X.1980.tb00273.x.

Leschik, M., Heide, G., Frischat, G.H., Behrens, H., Wiedenbeck, M., Wagner, N., Heide, K., Geißler, H., Reinholz, U., 2004. Determination of H_2O and D_2O contents in rhyolitic glasses. Phys. Chem. Glasses 45, 238–251.

Li, M., Russell, J.K., Giordano, D., 2020. Temperature-Pressure-Composition Model for Melt Viscosity in the Dp-An-Ab System. Chem. Geol. https://doi.org/10.1016/j.chemgeo.2020.119895.

Lima, E.F., Philipp, R.P., Rizzon, G.C., Waichel, B.L., Rossetti, L.M.M., 2012. Sucessões Vulcânicas e Modelo de Alimentação e Geração de Domos de Lava Ácidos da Formação Serra Geral na Região de São Marcos-Antonio Prado (RS). Geol. USP. Sér. Cient. 12, 49–64.

Lima, E.F., Waichel, B.L., Rossetti, L.M.M., Sommer, C.A., Simões,M.S., 2018. Feeder systems of acidic lava flows from the Paraná-Etendeka Igneous Province in Southern Brazil and their implications for eruption style. J. S. Am. Earth Sci. 81, 1–9.

Luchetti, A.C.F., Gualda, G.R., Gravley, D., Nardy, A.J.R., 2018a. Textural evidence for highgrade ignimbrites formed by low-explosivity eruptions, Paraná Magmatic Province, Southern Brazil. J. Volcanol. Geoth. Res. 355, 87–97. https://doi.org/10.1016/j.jvolgeores.2017.04.012.

Luchetti, A.C.F., Nardy, A.J.R., Madeira, J., 2018b. Silicic, high- to extremely high-grade ignimbrites and associated deposits from the Paraná Magmatic Province, southern Brazil. J. Volcanol. Geoth Res. 355, 270–286. https://doi.org/10.1016/j.jvolgeores.2017.11.010355.

Marsh, J.S., Ewart, A., Milner, S.C., Duncan, A.R., Miller, R.M., 2001. The Etendeka Igneous Province: magma types and their stratigraphic distribution with implications for the evolution of the Paraná-Etendeka flood basalt province. B. Volcanol. 62, 464–486.

Milner, S.C., Duncan, A.R., Ewart, A., 1992. Quartz latite rheoignimbrite flows of the Etendeka Formation, North-Western Namibia. B. Volcanol 54 (3), 200–219.

Milner, S.C., Duncan, A.R., Whittingham, A.M., Ewart, A., 1995. Trans-Atlantic correlation of eruptive sequences and individual silicic volcanic units within the Paraná-Etendeka igneous province. J. Volcanol. Geoth. Res 69 (3), 137–157.

Nardy, A.J.R., Machado, F.B., Oliveira, M.A.F., 2008. As rochas vulcânicas mesozóicas ácidas da Bacia do Paraná: litoestratigrafia e considerações geoquímico-estratigráficas. Rev. Bras. Geoc. 38 (1), 178–195. https://doi.org/10.25249/0375-7536.2008381178195.

Nowak, M., Behrens, H., 1997. An experimental investigation on diffusion of water in haplogranitic melts. Contrib. Mineral. Petrol. 126, 365–376.

Owen-Smith, T.M., Ashwal, L.D., Sudo, M., Trumbull, R.B., 2017. Age and Petrogenesis of the Doros Complex, Namibia, and Implications for early Plume-derived Melts in the Paraná–Etendeka LIP. J. Petrol. 58, 423–442. https://doi.org/10.1093/petrology/egx021.

Papale, P., 1999. Strain-induced magma fragmentation in explosive eruptions. Nature 397, 425–428.

Peate, D.W., 1997. The Paraná-Etendeka Province. In: Mahoney, J.J., Coffin, M.F. (Eds.), Large igneous provinces: continental, oceanic and planetary flood volcanism. Geophysical Monograph 100, American Geophysical Union (AGU), pp. 217–245.

Peate, D.W., Hawkesworth, C.J., Mantovani, M.S.M., 1992. Chemical stratigraphy of the Paraná lavas (S. America): classification of magma types and their spatial distribuition. B. Volcanol. 55, 119–139.

Pocklington, H.C., 1940. Rough measurement of high viscosities. P. Camb. Philos. Soc. 36, 507–508.

Polacci, M., Papale, P., Del Seppia, D., Giordano, D., Romano, C., 2004. Dynamics of Magma Ascent and Fragmentation in Trachytic Versus Rhyolitic Eruptions. J. Volcanol. Geoth. Res. 131, 93–108.

Polo, L.A., Janasi, V.A., 2014. Volcanic stratigraphy of intermediate to acidic rocks in southern Paraná Magmatic Province. Brazil. Geol. USP. Sér. Cient. 14, 83–100. https://doi.org/10.5327/Z1519-874X201400020005.

Polo, L.A., Giordano, D., Janasi, V., Freitas-Guiaraes, L., 2018a. Effusive silicic volcanism in in the Paraná Magmatic Province, South Brazil: Physico-chemical conditions of storage and eruption and considerations on the rheological behaviour during emplacement. J. Volcanol. Geoth Res. 355, 115–135. https://doi.org/10.1016/j.jvolgeores.2017.05.027.

Polo, L.A., Janasi, V., Giordano, D., Canon Tapia, E., Lima, E., Roverato, M., 2018b. Effusive silicic volcanism in the Paraná Magmatic Province, South Brazil: evidence for local fed lava flows and domes from detailed field work. J. Volcanol. Geoth. Res. 355, 204–218. https://doi.org/10.1016/j.jvolgeores.2017.08.007.

Roisenberg, A., Viero, A.P., 2000. O vulcanismo Mesozóico da Bacia do Paraná no Rio Grande do Sul. In: Holz, M., De Ros, L.F. (Eds.), Geologia Do Rio Grande Do Sul. CIGO/UFRGS, 444 p.

Romine, W.L., Whittington, A.G., 2015. A simple model for the viscosity of rhyolites as a function of temperature, pressure and water content, 170, pp. 281–300.

Rossetti, L., Lima, E.F., Waichel, B.L., Hole, M.J., Simões, M.S., Scherer, C.M.S., 2017. Lithostratigraphy and volcanology of the Serra Geral Group, Paraná-Etendeka Igneous Province in Southern Brazil: towards a formal stratigraphical framework. J. Volcanol. Geotherm. Res. 355, 98–114. https://doi.org/10.1016/j.jvolgeores.2017.05.008.

Roverato M; Giordano D; Echeverri-Misas C.M. Juliani C., 2016. Paleoproterozoic felsic volcanism of the Tapajós Mineral Province, Southern Amazon Craton, Brazil. J. Volcanol. Geoth. Res. 310, 98–106.

Roverato, M., Giordano, D., Giovanardi, T., Juliani, C., Polo, L.A., 2019. The 2.0-1.88 Ga Paleoproterozoic evolution of the southern Amazonian Craton (Brazil): an interpretation inferred by lithofaciological, geochemical and geochronological data. Gondwana Res. 70, 1–24.

Russell J.K., Giordano D., Hess K.U and Dingwell D.B., 2002. Modelling the non-Arrhenian rheology of silicate melts: numerical considerations. Eur. J. Mineral. 14, 417–427.

Russell, J.K., Giordano, D., Dingwell, D.B., 2003. High-temperature limits on viscosity of non-Arrhenian silicate melts. Am. Mineral. 88, 1390–1394.

Simões, M.S., Lima, E.F., Sommer, C.A., Rossetti, L.M.M., 2018a. Structures and lithofacies of inferred silicic conduits in the Paraná-Etendeka LIP, southernmost Brazil. J. Volcanol. Geoth. Res. 355, 319–336. https://doi.org/10.1016/j.jvolgeores.2017.12.013.

Simões, M.S., Lima, E.F., Sommer, C.A., Rossetti, L.M.M., 2018b. The Mato Perso Conduit System: evidence of silicic magma transport in the Paraná-Etendeka LIP. Braz. J. Geol. doi. https://doi.org/10.1590/2317-4889201820170080.

Sparks, R.S.J., Aspinall, W.P., 2004. Volcanic activity: Frontiers and challenges in forecasting, prediction and risk assessment. State of the Planet: Frontiers and Challenges in Geophysics 150, 359–373.

Stevenson, R.J., Dingwell, D.B., Webb, S.L., Sharp, T.G., 1996. Viscosity of microlite-bearing rhyolitic obsidians: an experimental study. Bull. Volcanol. 58, 298–309.

Takeuchi, S., 2011. Preeruptive magma viscosity: an important measure of magma eruptibility. J. Geophys. Res. 116, B10201 https://doi.org/10.1029/2011JB008243.

Tammann, G., Hesse, W., 1926. The dependency of viscosity on temperature in hypothermic liquids. Z. Anorg. Allg. Chem. 156.
Thiede, D.S., Vasconcelos, P.M., 2010. Parana flood basalts: rapid extrusion hypothesis confirmed by new $^{40}Ar/^{39}Ar$ results. Geology 38 (8), 747–750.
Tobolsky, A.V., Taylor, R.B., 1963. Viscoelastic Properties of a simple Organic Glass. J. Phys. Chem. 67, 2439–2442.
Tuffen, H., James, M.R., Castro, J.M., Schipper, C.I., 2013. Exceptional mobility of an advancing rhyolitic obsidian flow at Cordón Caulle volcano in Chile. Nat. Commun. 4, 2709. https://doi.org/10.1038/ncomms3709.
Umann, L.V., Lima, E.F., Sommer, C.A., De Liz, J.D., 2001. Vulcanismo ácido da região de Cambará do Sul-RS: litoquímica e discussão sobre a origem dos depósitos. Rev. Bras. Geosci. 31, 357–364. https://doi.org/10.5327/rbg.v31i3.950.
Vogel, H., 1921. The temperature dependence law of the viscosity of fluids. Phys. Z. 22, 645–646. https://doi.org/10.1146/annurev.fluid.39.050905.110207.
Waichel, B.L., de Lima, E.F., Viana, A.R., Scherer, C.M., Bueno, G.V., Dutra, G., 2012. Stratigraphy and volcanic facies architecture of the Torres Syncline, Southern Brazil, and its role in understanding the Paraná–Etendeka Continental Flood Basalt Province. J. Volcanol. Geoth. Res. 215, 74–82.
Whittingham, A.M., 1991. Stratigraphy and Petrogenesis of the Volcanic Formations Associated with the Opening of the South Atlantic, Southern Brazil. Ph.D. Thesis. University of Oxford, Oxford, UK.